IOWA STATE UNIVERSITY
Digital Repository

Retrospective Theses and Dissertations

Iowa State University Capstones, Theses and Dissertations

1952

Approximation of servomechanism transient response

Charles Holcomb Dawson
Iowa State College

Follow this and additional works at: https://lib.dr.iastate.edu/rtd

 Part of the Electrical and Electronics Commons

Recommended Citation
Dawson, Charles Holcomb, "Approximation of servomechanism transient response " (1952). *Retrospective Theses and Dissertations*. 13287.
https://lib.dr.iastate.edu/rtd/13287

This Dissertation is brought to you for free and open access by the Iowa State University Capstones, Theses and Dissertations at Iowa State University Digital Repository. It has been accepted for inclusion in Retrospective Theses and Dissertations by an authorized administrator of Iowa State University Digital Repository. For more information, please contact digirep@iastate.edu.

www.manaraa.com

NOTE TO USERS

This reproduction is the best copy available.

UMI®

APPROXIMATION OF SERVOMECHANISM TRANSIENT RESPONSE

by

Charles H. Dawson

A Dissertation Submitted to the

Graduate Faculty in Partial Fulfillment of

The Requirements for the Degree of

DOCTOR OF PHILOSOPHY

Major Subject: Electrical Engineering

Approved:

Signature was redacted for privacy.
In Charge of Major Work

Signature was redacted for privacy.
Head of Major Department

Signature was redacted for privacy.
Dean of Graduate College

Iowa State College

1952

UMI Number: DP12405

INFORMATION TO USERS

The quality of this reproduction is dependent upon the quality of the copy submitted. Broken or indistinct print, colored or poor quality illustrations and photographs, print bleed-through, substandard margins, and improper alignment can adversely affect reproduction.

In the unlikely event that the author did not send a complete manuscript and there are missing pages, these will be noted. Also, if unauthorized copyright material had to be removed, a note will indicate the deletion.

UMI®

UMI Microform DP12405

Copyright 2005 by ProQuest Information and Learning Company.

All rights reserved. This microform edition is protected against unauthorized copying under Title 17, United States Code.

ProQuest Information and Learning Company
300 North Zeeb Road
P.O. Box 1346
Ann Arbor, MI 48106-1346

TK3226
D33s

TABLE OF CONTENTS

T10396 ✓

INTRODUCTION

The term "Servomechanism"*, as used herein, is defined as

> a control system which tends to maintain a prescribed relationship of one system variable to another by comparing functions of these variables and using the difference as a means of control.[1](p. 909)

The symbolism to be used herein is essentially that introduced by Brown and Campbell[2]. The symbols are briefly defined when first used and a full listing is included in Appendix I.

The ideal servomechanism is, of course, one in which the input and output are always in the proper relationship to one another but this ideal has not been and cannot be obtained. Rather the designer must attempt to produce at reasonable cost a device having acceptable deviations between input and output. Such deviations actually occur as functions of time when the input is subjected to random variations. However, the design specification is likely to prescribe the allowable output behavior corresponding to special inputs such as the unit impulse or unit step.

Although the design criterion is thus in the time domain, the effect of parameter variations in all but the simplest cases is obscure

---

*The A.I.E.E. Feedback Control Systems Committee has proposed that the term "servomechanism" be restricted to such of the above systems as have mechanical position as the controlled variable.

when classical mathematical methods are used to solve the differential equations defining system behavior. The usual technique is then that of operational or transform mathematics. The facts that these methods, under very general assumptions, lead to expressions entirely similar to those of alternating-current steady-state frequency analysis and that a very large background of frequency design information exists have led to the use of the frequency domain in servomechanism design. Such design methods lead directly to adequate stability criteria through the work of Nyquist[3] and Bode[4]. They do not, however, lead easily to a knowledge of the transient response of the completed system despite the existence of mathematical methods which transform from the frequency to the time domain.

These mathematical methods, which are applicable to linear systems, involve integration over the complete frequency spectrum and do not, except in very specific and elementary cases, lead to closed expressions for the time response. Since even completely random inputs may be considered as composed of successions of impulses or steps and since the impulse response can be easily derived from the step response and vice versa, all methods of surmounting this obstacle in the literature are concerned with either impulse or step response. Also, because initial energy storage can generally be treated as an additional input, all methods in the literature assume zero initial energy storage.

The methods of approximating step response due to Bedford and Fredendall[5], Chestnut and Mayer[6], and Harris, Kirby, and von Arx[7] and those of approximating impulse response due to Wheeler[8] and Floyd[9]

will be discussed individually.

Bedford and Fredendall assume that the sinusoidal frequency response, $H(\omega)$, is known in both magnitude and angle at all frequencies. They assume that the step response will be equivalent to that due to a square wave input whose half period is longer than the settling time of the step response. The square wave input is then analyzed into its Fourier series components, the response to each is determined using the known $H(\omega)$ and the results combined to give the step response. While this method leads to any desired degree of accuracy, the proper square wave period is difficult to select since too short a period will not exceed twice the settling time and too long a period will introduce a large number of low frequency Fourier terms resulting in extra computation. Hence at least two trials would appear necessary before the computation could be completed.

$$\theta_i(t) = \frac{4}{\pi} \sum_{n=1}^{\infty} \frac{1}{2n-1} \sin(2n-1) \frac{2\pi t}{T}$$

where T is the period of the input signal, $\theta_i(t)$.

$$H(\omega) = M(\omega) e^{j\varphi(\omega)}$$

$$\theta_o(t) = \frac{4}{\pi} \sum_{n=1}^{\infty} \frac{M(2n-1)\frac{2\pi}{T}}{2n-1} \sin\left\{\left[(2n-1)\frac{2\pi t}{T}\right] + \varphi\left[(2n-1)\frac{2\pi}{T}\right]\right\}$$

where $\theta_o(t)$ is the output response.

These authors have also applied a very similar procedure to the determination of the impulse response using a repetitive input signal

consisting of a short pulse followed by a dead period exceeding the settling time of the response.[10]

The Chestnut and Mayer method does not give the step response as a function of time but correlates certain features of the frequency and time responses. Systems are considered whose open-loop response, $KG(\omega)$, has the form shown in Figure 1(a); the slope below ω_1 is 6 db per octave and the gain at ω_1 is μ_1; the slope between ω_2 and ω_3 is again 6 db per octave with 0 db occurring at ω_0. The slopes between ω_1 and ω_2 and above ω_3 together with μ_1 are considered as parameters characterizing the system. A series of charts is presented with μ_1 and these two slopes as parameters which relate the salient points of the closed-loop frequency response, namely, the peak value of $M(\omega)$* and the frequency at which it occurs (see Figure 1(b)), with the salient points of the closed-loop time response to an input step, namely, the peak value of the output, the time at which it occurs, the settling time, and the period of the lowest oscillation frequency (see Figure 1(c)).

Although the charts are derived for a 6 db slope below ω_1, other values of this slope have been found to give essentially the same response; hence the charts may be used for other slopes. Since the charts may be entered from either the time or frequency data, they should be particularly useful in determining the type of frequency response needed to give a specified step response.

---

*$M(\omega)$ is the absolute value of $H(\omega)$.

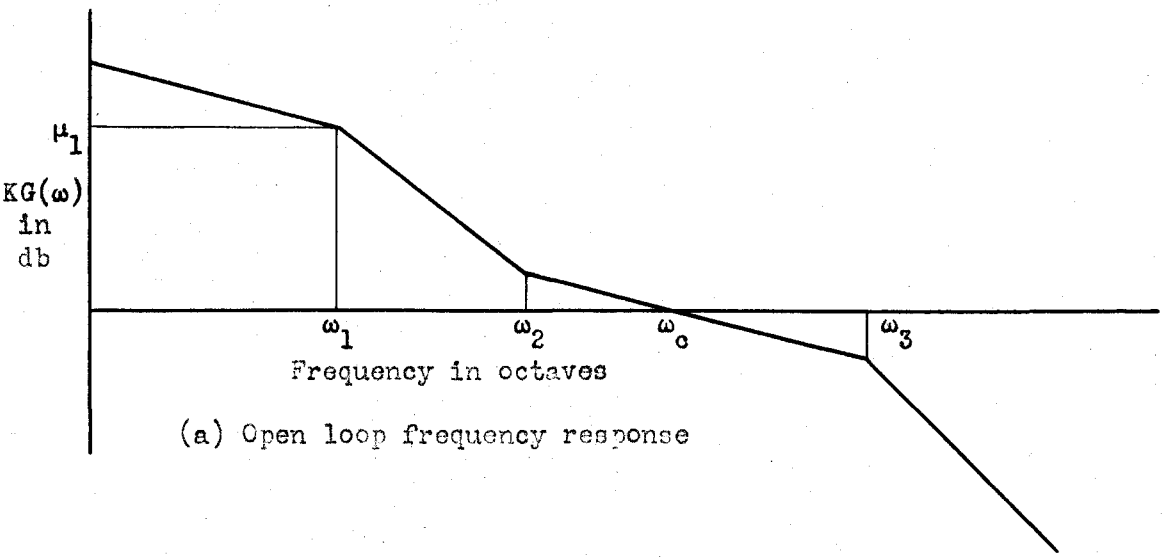

(a) Open loop frequency response

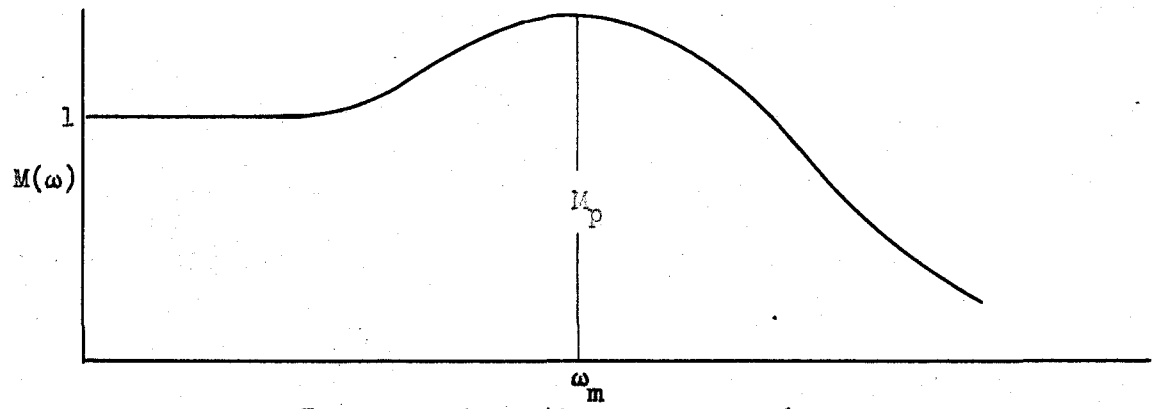

(b) Closed loop frequency response

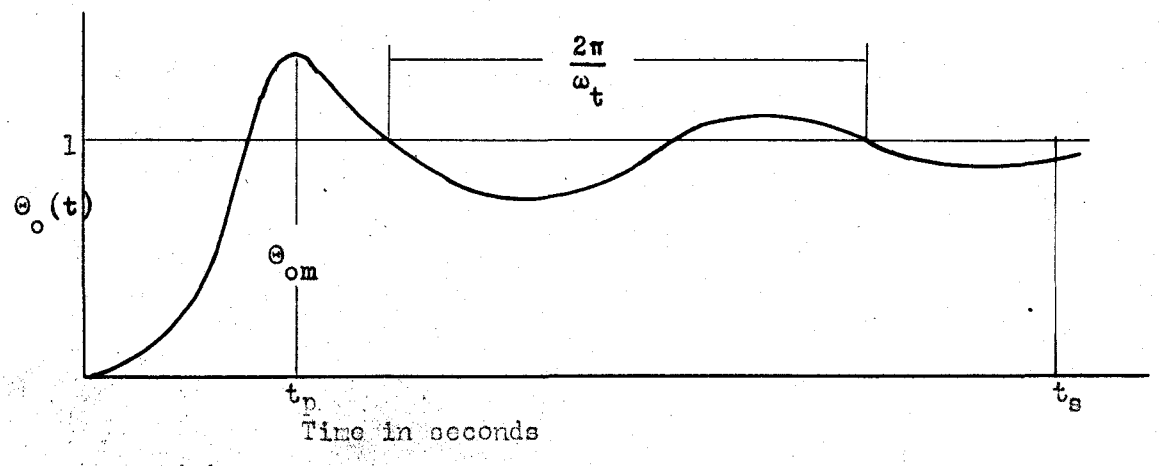

(c) Step response

Figure 1 Chestnut and Mayer Symbolism

Harris, Kirby, and von Arx consider systems for which $KG(\omega) = \frac{\theta_o}{\mathcal{E}}(\omega)$* consists of four straight line sections on a decibel-frequency plot, ω_o (where db = 0) occurring between ω_2 and ω_3 as in Figure 1(a). $\frac{\theta_i}{\mathcal{E}}$ is then approximated as equal to $KG(\omega)$ below ω_o and as unity above ω_o.

$$KG(\omega) = \frac{\theta_o}{\mathcal{E}}(\omega) = \omega_3\omega_o \frac{(s+\omega_2)}{s(s+\omega_1)(s+\omega_3)}$$

$$\text{Approximate } \frac{\theta_i}{\mathcal{E}}(\omega) = \frac{(s+\omega_2)(s+\omega_o)}{s(s+\omega_1)}$$

The expression for $\frac{\theta_i}{\mathcal{E}}$ is solved by the usual Laplace transform methods to give $\mathcal{E}(t)$ for any specified $\theta_i(t)$. However, the approximate $\frac{\theta_i}{\mathcal{E}}(\omega)$ is not valid near ω_o and a constant correction factor, R, is required in the range $\frac{1}{\omega_o} \leq t \leq \frac{1}{\omega_2}$; R is evaluated as the ratio of the approximate $\frac{\theta_i}{\mathcal{E}}(\omega_o)$ to the exact $\frac{\theta_i}{\mathcal{E}}(\omega_o) = 1 + \frac{\theta_o}{\mathcal{E}}(\omega_o)$. The response is then $R \times \mathcal{E}(t)$ for $\frac{1}{\omega_o} \leq t \leq \frac{1}{\omega_2}$ and $\mathcal{E}(t)$ elsewhere. The reference contains results of this method for a variety of $KG(\omega)$ slope characteristics. The examples shown, however, do not indicate very close agreement between predicted and exact results.

In Wheeler's method of paired echoes, the impulse response, h(t), of an idealized system

$$M(\omega) = K \qquad \omega < \omega_o$$

$$M(\omega) = 0 \qquad \omega > \omega_o$$

and $$\varphi(\omega) = a\omega$$

is first determined in the usual $Si(t) = \frac{\sin(t-a)}{t-a}$ form and this response

---

* $\mathcal{E}$ is the error, defined as the input minus the output.

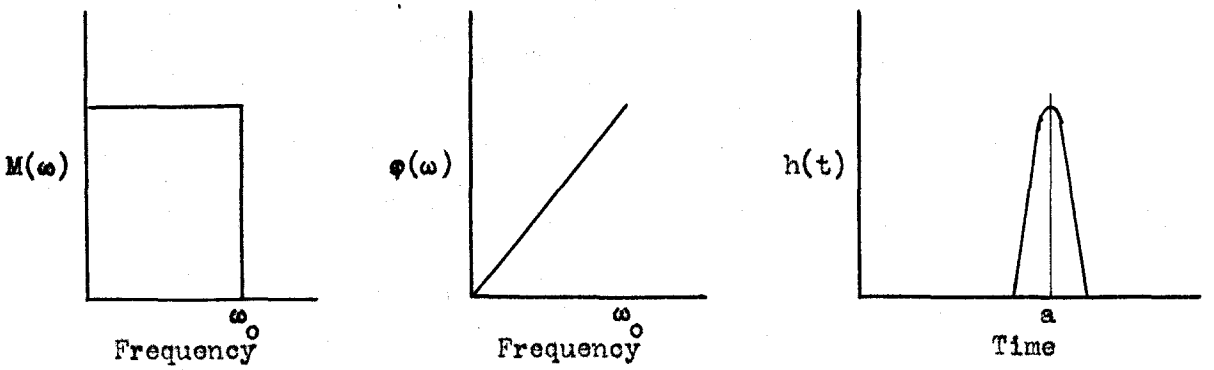

(a) Idealized system

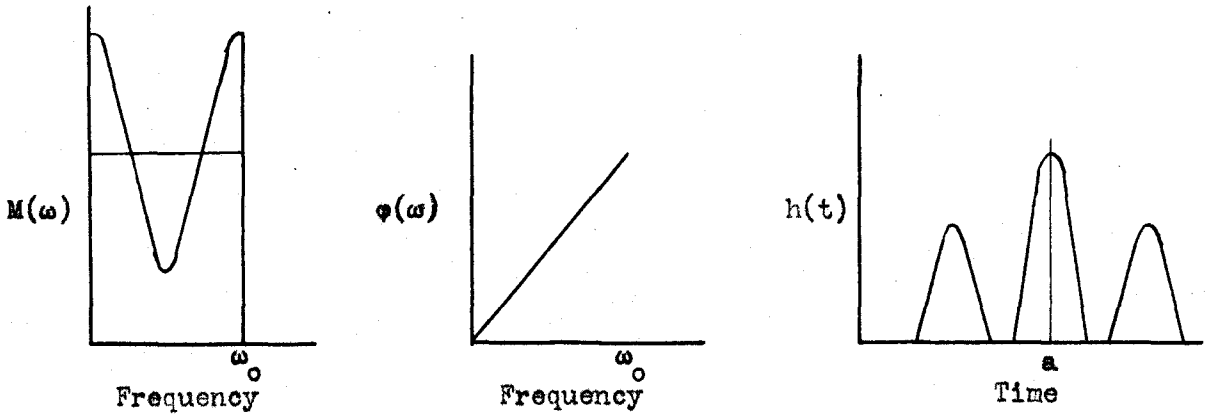

(b) Magnitude distortion

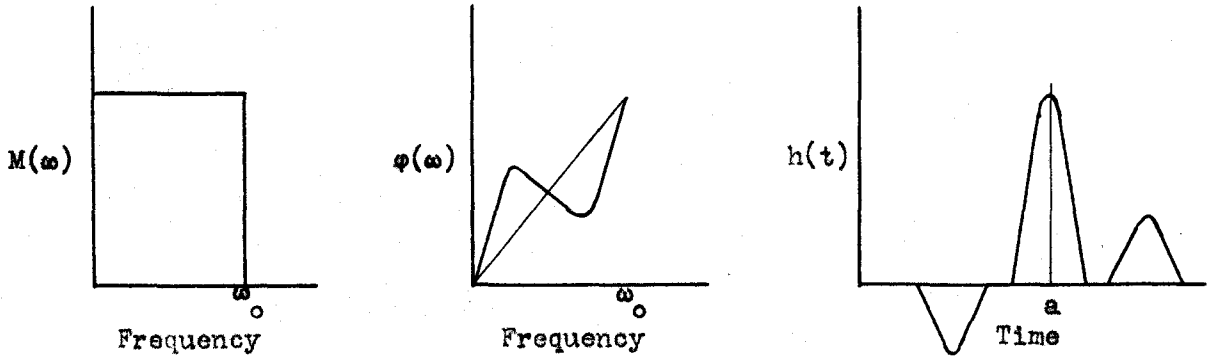

(c) Phase distortion

Figure 2 Method of Paired Echoes

(see Figure 2(a)) is taken as the basic unit. Deviations of $M(\omega)$ from the above ideal form are analyzed as Fourier components leading to pairs of positive echoes, each having the same shape as the basic response, one occurring before it and one after it as shown in Figure 2(b). Deviations of $\varphi(\omega)$ from its ideal form lead to pairs of negative echoes as shown in Figure 2(c). The basic response and all echoes are then added together to give the impulse response, $h(t)$, for the actual system. Due to certain assumptions in the derivation, large deviations from ideal characteristics must be handled as the sum of a number of small deviations.

The method developed by Floyd and that to be presented herein are both based on the following widely known analysis of the inverse Laplace transform. Assuming that $H(s)$ has no poles in the right half plane, which is necessarily true of all stabilized systems, and that the system is linear, the general inverse Laplace transform* reduces to

$$h(t) = \frac{1}{2\pi} \int_{-\infty}^{+\infty} H(\omega) e^{j\omega t} d\omega \ , \qquad (1)$$

but $$H(\omega) = R(\omega) + jI(\omega) \qquad (2)$$

---

*These results can equally well be derived from the inverse Fourier transform.

where $R(-\omega) = R(\omega)$ and $I(-\omega) = -I(\omega)$

and $$e^{j\omega t} = \cos \omega t + j \sin \omega t \qquad (3)$$

where $\cos(-\omega t) = \cos \omega t$ and $\sin(-\omega t) = -\sin \omega t$

$$h(t) = \frac{1}{2\pi} \int_{-\infty}^{+\infty} \left[R(\omega) \cos \omega t - I(\omega) \sin \omega t\right] +$$

$$j \left[R(\omega) \sin \omega t + I(\omega) \cos \omega t\right] d\omega \, . \qquad (4)$$

Since $R(\omega) \sin \omega t$ and $I(\omega) \cos \omega t$ are both odd functions of ω, the integral of their sum over the range $-\infty$ to $+\infty$ is zero. Therefore

$$h(t) = \frac{1}{2\pi} \int_{-\infty}^{+\infty} \left[R(\omega) \cos \omega t - I(\omega) \sin \omega t\right] d\omega \qquad (5)$$

Since $R(\omega) \cos \omega t$ and $I(\omega) \sin \omega t$ are both even functions of ω, the integral of their difference over the same range is twice that over the range 0 to $+\infty$

$$h(t) = \frac{1}{\pi} \int_{0}^{\infty} R(\omega) \cos \omega t \, d\omega - \frac{1}{\pi} \int_{0}^{\infty} I(\omega) \sin \omega t \, d\omega$$

$$= h_r(t) + h_i(t) \qquad (6)$$

where $h_r(-t) = h_r(t)$ and $h_i(-t) = -h_i(t)$

since the integrals are respectively even and odd functions of time. Since for all negative values of time, a physical system can show no response to an input impulse occurring at $t = 0$

$$h(-t) = h_r(-t) + h_i(-t) = h_r(t) - h_i(t) = 0 \, . \qquad (7)$$

Therefore

$$h_r(t) = h_i(t)$$

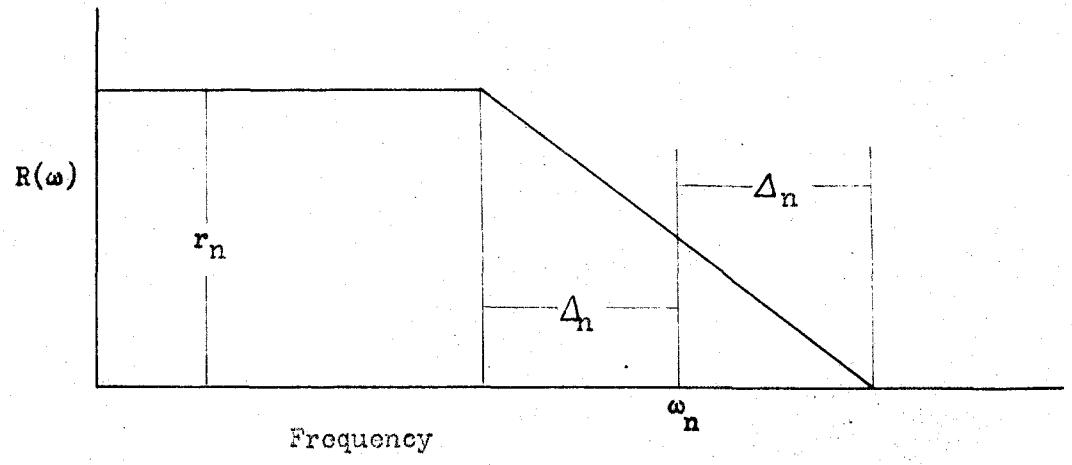

(a) Typical trapezoid

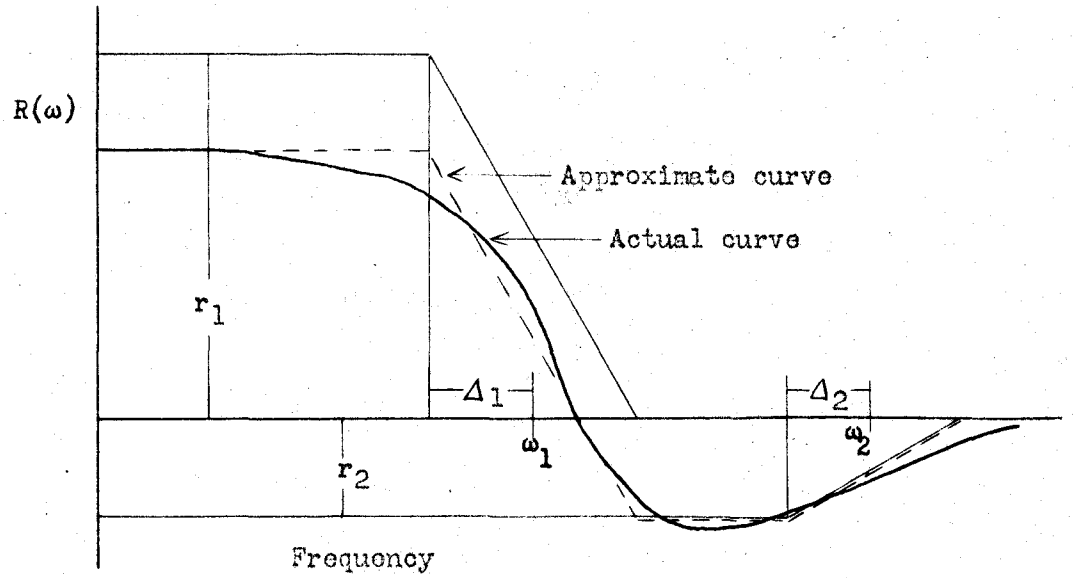

(b) Method of approximation

Figure 3 Floyd's Approximation

and $$h(t) = \frac{2}{\pi} \int_0^\infty R(\omega) \cos \omega t \, d\omega \qquad (8)$$

or $$h(t) = -\frac{2}{\pi} \int_0^\infty I(\omega) \sin \omega t \, d\omega \qquad (9)$$

Floyd uses Equation (8) as the basis of his method. By superimposing loci of constant R, where $R(\omega)$ is the real part of $H(\omega)$, on the plot of KG (ω) in either polar or log modulus vs angle coordinates, a plot of $R(\omega)$ vs ω is obtained. From the plot, $R(\omega)$ is approximated by a number of trapezoids of the form shown in Figure 3(a) in the manner shown by Figure 3(b), each trapezoid being characterized by three parameters: r_n, Δ_n, and ω_n. The $h_n(t)$ corresponding to each of these trapezoids is obtained by solving Equation (8) to give

$$h_n(t) = \frac{2r_n\omega_n}{\pi} \left(\frac{\sin \omega_n t}{\omega_n t}\right)\left(\frac{\sin \Delta_n t}{\Delta_n t}\right).$$

Although only a relatively small number of trapezoids are needed to give excellent agreement between predicted and exact curves of h(t) in the examples presented by Floyd, the labor involved is very large since each term of the series for h(t) contains the product of $\sin \omega_n t$ and $\sin \Delta_n t$.

Despite the merits of these methods for the specific problems for which they were developed, none seems to provide a method giving a high degree of accuracy without involving much tedious computation. It is believed that the method to be presented herein does give highly acceptable accuracy and requires less computation than those described above.

THE PROPOSED METHOD

The problem, to restate, is, being given the variation of the vector $KG(\omega)$ as a function of frequency, in either analytical or graphical form, for a linear servomechanism having a satisfactory degree of stability, to predict the system response $\theta_o(t)$ for an arbitrary input $\theta_i(t)$. The steps of the proposed method are:

a. Derive a plot of $I(\omega)^*$ vs ω from the given $KG(\omega)$.

b. Select a cutoff frequency ω_o such that $I(\omega)$ may be assumed equal to zero for $\omega > \omega_o$. ω_o is the frequency equal empirically to 1.3 times the frequency, $\omega_{.1}$, at which $I(\omega) = -.1$ and is decreasing in absolute value.

c. Assume that $I(\omega)$ decreases linearly from $\omega_{.1}$ where $I(\omega) = -.1$ to zero at ω_o and express $I(\omega)$ as a Fourier sine series in the interval $0 < \omega < \omega_o$,

$$I(\omega) = \sum_{n=1}^{\infty} a_n \sin \frac{n\omega}{\omega_o} \qquad 0 < \omega < \omega_o$$

$$= 0 \qquad \omega > \omega_o \qquad (10)$$

---

*$I(\omega)$ is the imaginary component of $H(\omega)$.

d. Take $h(t) = 2\omega_0 \sin \tau \sum_{n=1}^{\infty} n(-1)^n \frac{a_n}{n^2\pi^2 - \tau^2}$ (11)

where $\tau = \omega_0 t$.

e. Then $\theta_0(t) = \int_0^t h(t-x)\,\theta_1(x)\,dx$ (12)

In the cases investigated, retention of only four terms of the series for h(t) gave excellent agreement with exact curves. It should be noted that Equation (11) lends itself to rapid computation since, inside the summation sign, time occurs only in the τ^2 term and even there is the same for all n. A form for use in this computation is included in Appendix II.

Suppose $KG(\omega)$ is given as a plot in the KG plane (Nyquist diagram). Let $KG(\omega) = x + jy$ (13)

Then $$H(\omega) = \frac{KG(\omega)}{1+KG(\omega)} = \frac{x+jy}{(1+x)+jy} = \frac{(x+jy)([1+x]-jy)}{(1+x)^2+y^2}$$

$$= \frac{[x(1+x)+y^2]+jy[1+x-x]}{(1+x)^2+y^2} . \quad (14)$$

But $$I(\omega) = \mathcal{J} H(\omega) = \frac{y}{(1+x)^2+y^2} . \quad (15)$$

The locus for $I(\omega)$ equaling a constant, say I, is then

$$I = \frac{y}{(1+x)^2+y^2} \quad \text{or} \quad (x+1)^2+y^2-\frac{y}{I} = 0 .$$

Completing the square on y yields

$$(x+1)^2 + (y - \frac{1}{2I})^2 = (\frac{1}{2I})^2 \quad (16)$$

which is a circle of radius 1/2I with its center at x = -1, y = 1/2I. Consider the point (-1,0); this point satisfies Equation (16) for all

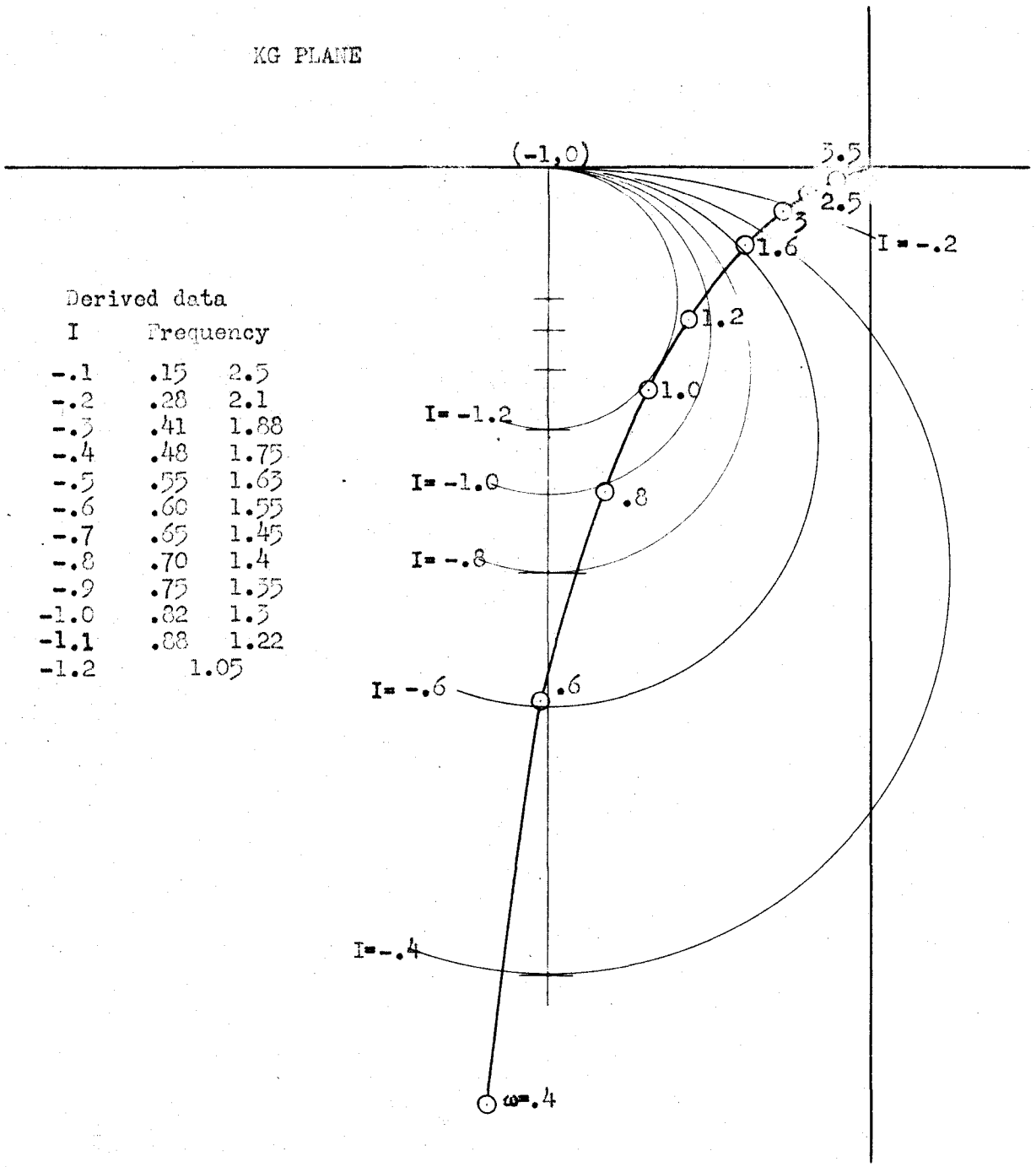

Derived data

I	Frequency	
-.1	.15	2.5
-.2	.28	2.1
-.3	.41	1.88
-.4	.48	1.75
-.5	.55	1.63
-.6	.60	1.55
-.7	.65	1.45
-.8	.70	1.4
-.9	.75	1.35
-1.0	.82	1.3
-1.1	.88	1.22
-1.2	1.05	

Figure 4 Loci of Constant I on the KG Plane Superimposed on the Curve for $KG(\omega) = \frac{1.36}{j\omega(1+j\omega)}$

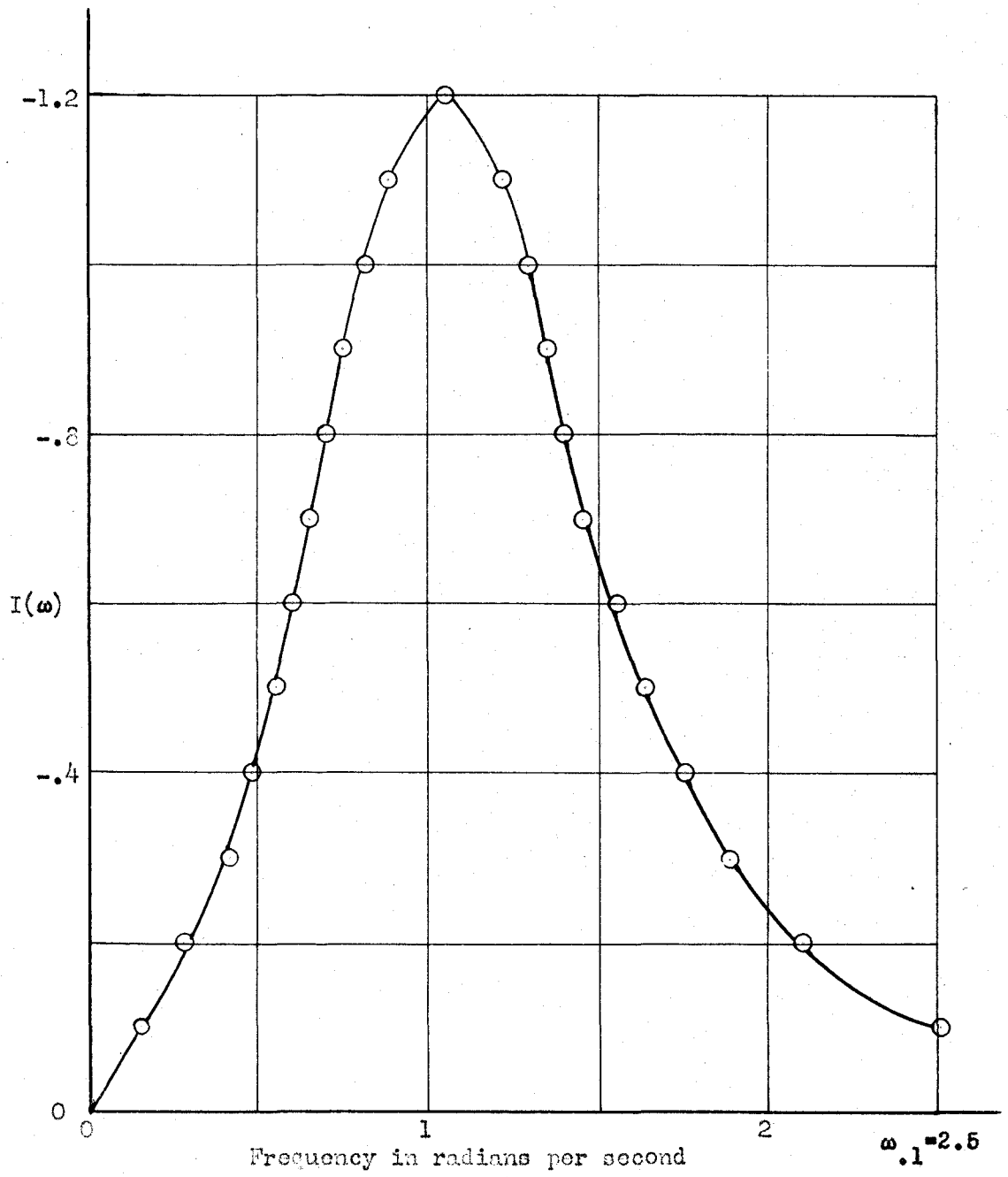

Figure 5 $I(\omega)$ vs ω for $KG(\omega) = \frac{1.36}{j\omega(1+j\omega)}$

values of I and hence all circles of this family pass through (-1,0). Several of these circles are shown in Figure 4 superimposed on a $KG(\omega)$ curve. The resulting $I(\omega)$ vs ω plot is given as Figure 5.

Suppose $KG(\omega)$ is given as a plot in the KG^{-1} plane where

$$KG^{-1}(\omega) = \frac{1}{KG(\omega)} = u + jv = \frac{1}{x+jy}$$

Then $$x + jy = \frac{u-jv}{u^2+v^2} \quad \text{and} \quad x^2 + y^2 = \frac{1}{u^2+v^2} \; . \tag{17}$$

Substituting Equation (17) into Equation (15) yields

$$I = \frac{y}{(1+x)^2+y^2} = \frac{-v}{u^2+v^2} \quad \frac{1}{1 + \frac{2u}{u^2+v^2} + \frac{1}{u^2+v^2}}$$

$$I(u^2 + v^2 + 2u + 1) = -v$$

$$(U + 1)^2 + (v + \frac{1}{2I})^2 = (\frac{1}{2I})^2 \; . \tag{18}$$

This is again a circle of radius $1/2I$ but with its center at $x = -1$, $y = -1/2I$; hence loci for positive values of I in the KG plane are loci for equal negative values of I in the KG^{-1} plane and vice versa. A plot of $I(\omega)$ vs ω for the KG^{-1} plane would be derived in a manner exactly similar to that shown in Figures 4 and 5 for the KG plane.

Finally, suppose $KG(\omega)$ is given as a plot of $KG(\omega)$ in decibels vs the angle of $KG(\omega)$ (lm-ang plane)*. Let $r^2 = x^2 + y^2$,

$$x = r \cos \varphi, \quad \text{and} \quad y = r \sin \varphi \tag{19}$$

Substituting Equation (19) in Equation (15) yields

---

*log modulus vs angle.

$$I = \frac{y}{1+2x+x^2+y^2} = \frac{r \sin \varphi}{1+2r \cos\varphi+r^2} \qquad (20)$$

In order to put Equation (20) into a form more suitable for computation, let (see Figure 6)

$$\alpha = 180^\circ - \tan^{-1} \frac{1}{2I}$$

Then $$\sin \alpha = \frac{1/2I}{\left[1+(\frac{1}{2I})^2\right]^{1/2}} = \frac{1}{\left[4I^2+1\right]^{1/2}}$$

$$\cos \alpha = -\frac{1}{\left[1+(\frac{1}{2I})^2\right]^{1/2}} = \frac{-2I}{\left[4I^2+1\right]^{1/2}}$$

$$I + 2rI \cos \varphi + Ir^2 = r \sin \varphi$$

$$I(r+\tfrac{1}{r}) = \sin \varphi - 2I \cos \varphi$$

$$\frac{I(r+\frac{1}{r})}{\left[4I^2+1\right]^{1/2}} = \frac{\sin \varphi}{(4I^2+1)^{1/2}} - \frac{\cos \varphi \, 2I}{(4I^2+1)^{1/2}}$$

$$= \sin \varphi \sin \alpha + \cos \varphi \cos \alpha = \cos\left[\pm(\varphi-\alpha)\right]$$

Therefore $$\varphi = \pm \cos^{-1} \frac{I(r+\frac{1}{r})}{(4I^2+1)^{1/2}} + \alpha$$

$$\varphi = 180^\circ - \tan^{-1} \frac{1}{2I} \pm \cos^{-1} \frac{(r+\frac{1}{r})}{\left[4+(\frac{1}{I})^2\right]^{1/2}} \qquad (21)$$

Consider $$\cos \beta = \frac{(r+\frac{1}{r})}{\left[4+(\frac{1}{I})^2\right]^{1/2}}$$

then $$-\sin \beta \frac{\partial \beta}{\partial r} = \frac{1}{\left[4+(\frac{1}{I})^2\right]^{1/2}} (1 - \frac{1}{r^2})$$

Therefore $\frac{\partial \beta}{\partial r} = 0$ when $r = 1$ and the maximum value of β is given by

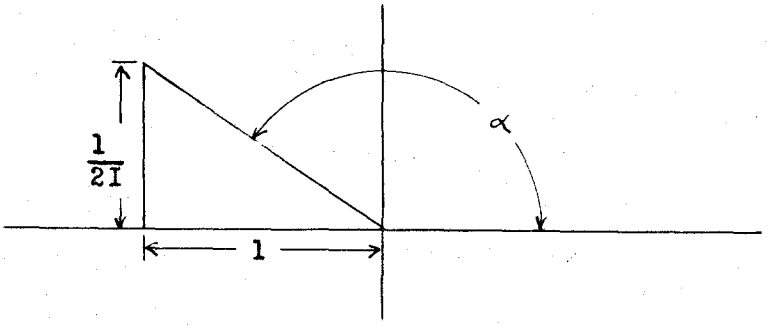

Figure 6 Definition of α

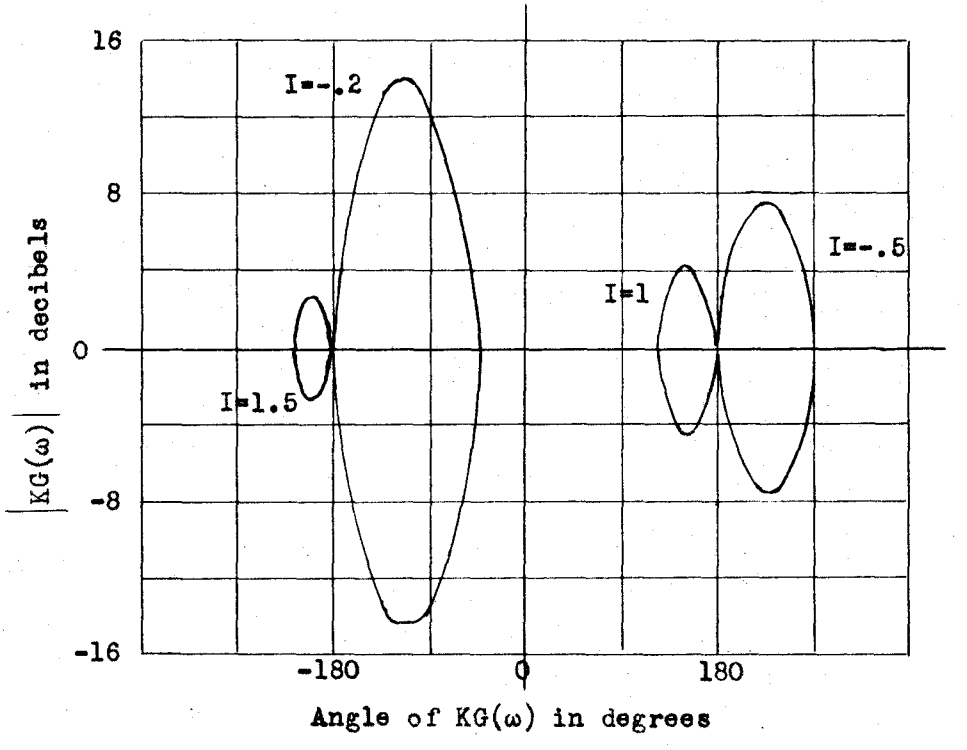

Figure 7 Loci of Constant I in the Lm-Ang Plane

$$\mathcal{B}_{max} = \cos^{-1} \frac{2}{\left[4+\left(\frac{1}{I}\right)^2\right]^{1/2}} = \cos^{-1} \frac{1}{\left[1+\left(\frac{1}{2I}\right)^2\right]^{1/2}} = \tan^{-1} \frac{1}{2I}$$

The minimum value, $\mathcal{B} = 0$, occurs when $r + \frac{1}{r} = \left(4 + \frac{1}{I^2}\right)^{1/2}$ which coincides with the maximum value of r. The limiting values of φ are therefore $\varphi = \pm 180^\circ$ and $\varphi = \pm 180^\circ - 2 \tan^{-1} \frac{1}{2I}$. These relations show that, as indicated in Figure 7, the locus of I is symmetrical about the zero db line (where $r = 1$) and about the lines $\varphi = \pm 180^\circ - \tan^{-1} \frac{1}{2I}$ (where r reaches its maximum). $I = 0$ corresponds to the lines $\varphi = 0$ and $\varphi = \pm 180^\circ$. An example of these loci and their application to a particular case are given in Figures 8 and 9.

The heart of the method is the matter of choosing a proper value of cutoff frequency, ω_o. If no assumptions were involved, integration over the full infinite range would yield exact answers for all values of time. As the range of integration is reduced, assuming only that $I(\omega) = 0$ for $\omega \geq \omega_o$, the results should remain excellent for some range of very large values of ω_o since $I(\omega)$ falls off rapidly with frequency. However, as ω_o is still further reduced, it must reach a value such that

$$\int_{\omega_o}^{\infty} I(\omega) \sin \omega t \, d\omega$$

is no longer negligibly small compared to

$$\int_{0}^{\omega_o} I(\omega) \sin \omega t \, d\omega.$$

This effect sets a lower limit on ω_o independent of the details of the

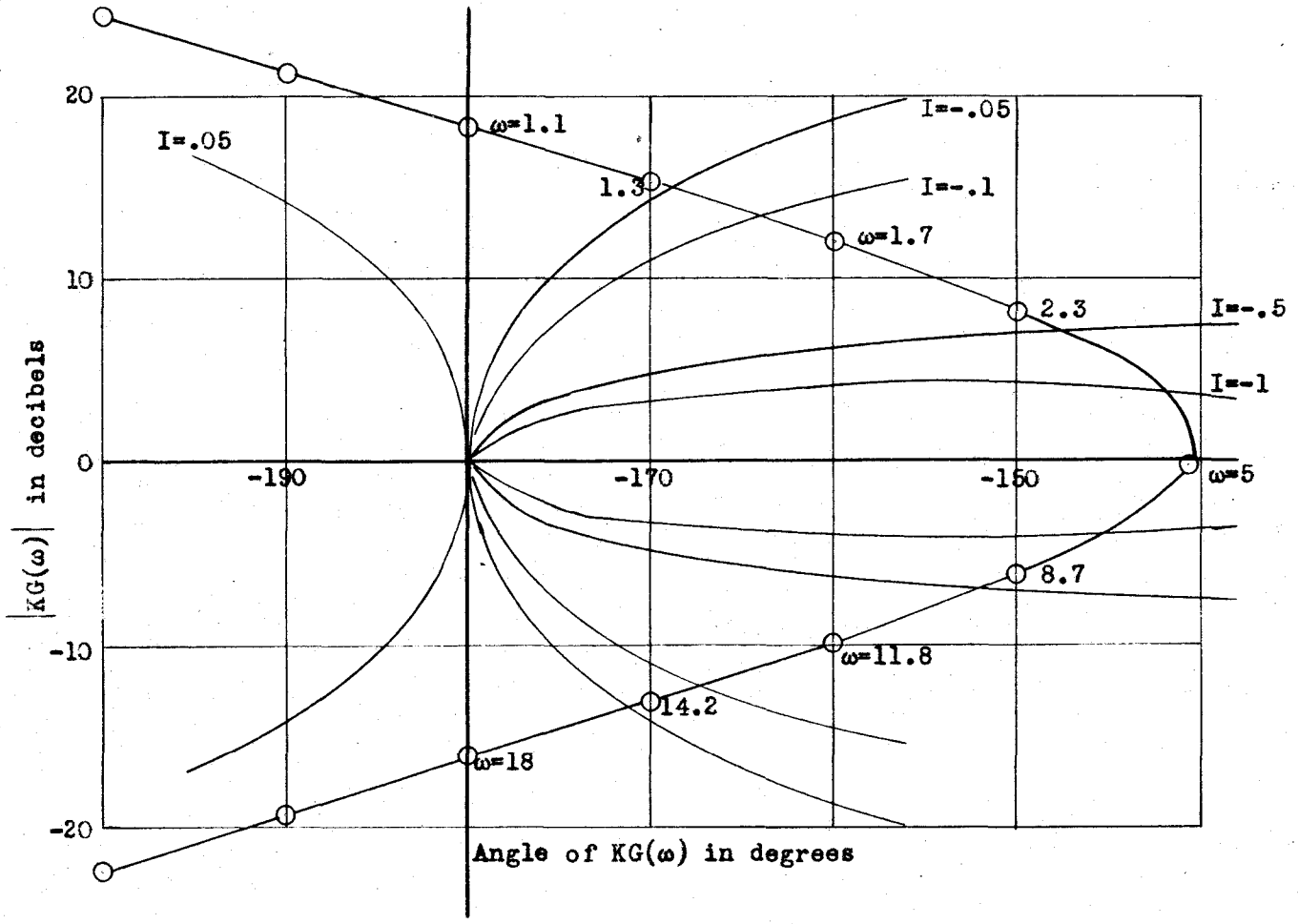

Figure 8 Loci of Constant I on the Lm-Ang Plane Superimposed on the Curve of $KG(\omega)=\frac{5(1+j\omega)^2}{(j\omega)^3(1+j.05\omega)^2}$

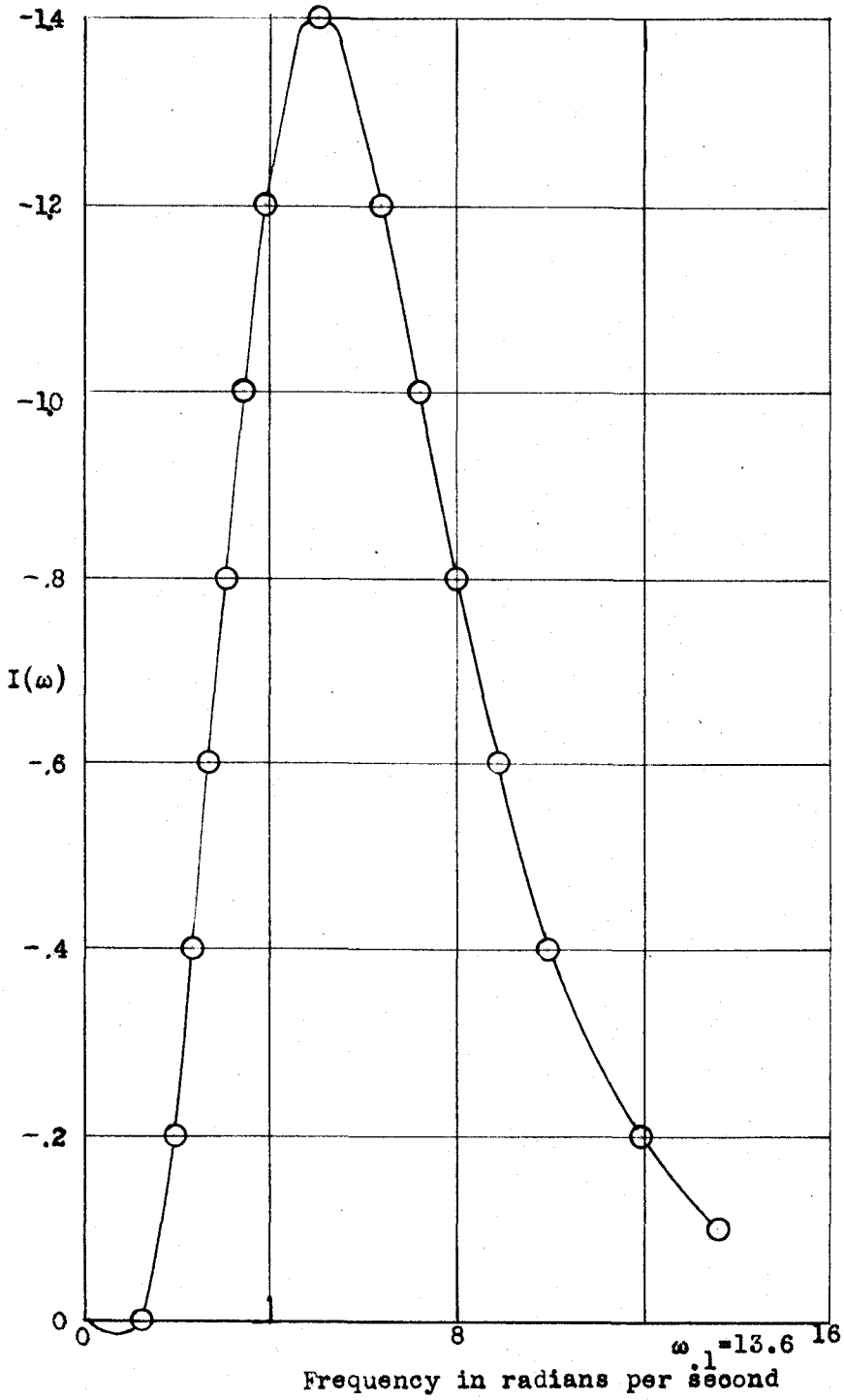

Figure 9 $I(\omega)$ vs ω for $KG(\omega)=\frac{5(1+j\omega)^2}{(j\omega)^3(1+j.05\omega)^2}$

assumptions of the method used to approximate h(t).

The three assumptions proposed herein are that $I(\omega)$ decreases linearly between $\omega_{.1}$ and ω_0, $I(\omega_0)$ being zero, that four terms of the Fourier sine series for $I(\omega)$ are adequate, and that the coefficients of these four terms can be found with sufficient accuracy by eighteen point graphical integration. As ω_0 is increased above its lower limiting value, a cutoff frequency will be reached which does not lie in the range in which all these assumptions may be considered valid. As these ranges of validity are not necessarily continuous and as the errors due to their invalidity are not necessarily all in the same direction, random behavior may be expected. Further consideration of these sources of error is given in the Discussion.

Since both the above integrals are functions of time, a general numerical ratio of their contributions to h(t) cannot be found even when the exact form of $I(\omega)$ is known analytically. Since the shape of $I(\omega)$ is also widely variable between systems, it is impossible even to compare the area cutoff above ω_0 with that retained in the general case. However, at certain times, corresponding to $\gamma = n\pi$, the series for h(t) reduces to a single term, $(-1)^n a_n \frac{\omega_0}{\pi}$, and it is possible to see how agreement at these singular points improves with increasing ω_0. Figure 10 shows how the values at $\gamma = \pi$ and 2π approach the exact curve of h(t) for Example 1 as ω_0 is increased, thus indicating the existance of the lower limit mentioned above.

In order to determine what value of ω_0 gave the "best" agreement with the exact response, an RMS error was used which was computed by

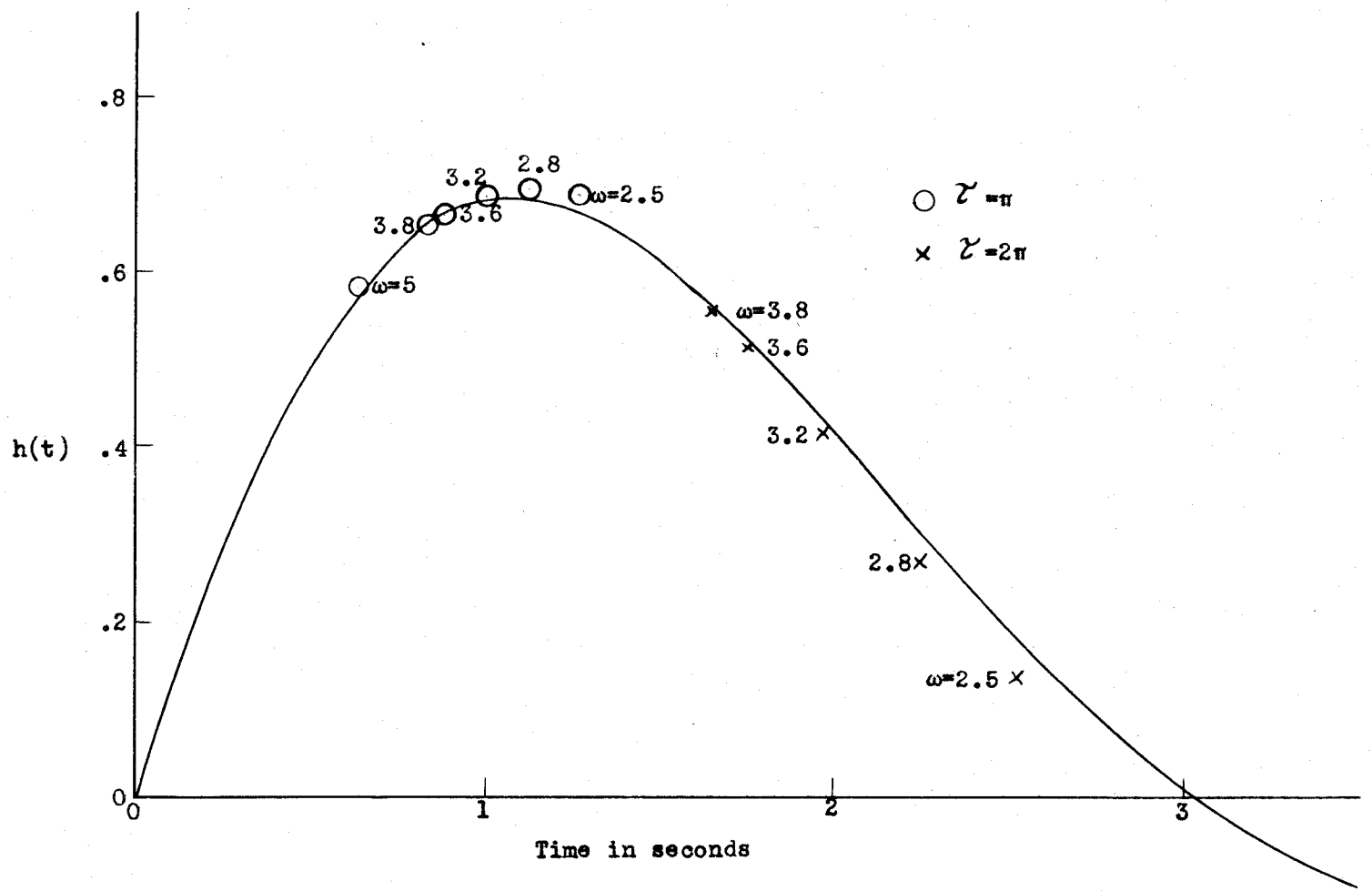

Figure 10 Effect of ω_o on Agreement at $\gamma = n\pi$ Points

taking the square root of the average of the squares of the differences between the predicted and exact responses at twenty points equally spaced over a convenient interval equal to or slightly greater than that of the first positive alternation of h(t). To establish a percentage reference, the same RMS error was computed assuming that a difference equal to one percent of the true h(t) existed at each of the twenty times.

As anticipated, the RMS error at first decreased quite rapidly with increasing ω_0 and then showed random behavior depending on which, if any, of the three error sources mentioned above became important. Figure 12 illustrates this behavior for the four examples.

In each example, a lower limit for ω_0 at which the RMS error was 5% was selected. Upper limits were also set at the 5% error points in Examples 2 and 4; however, the error in Examples 1 and 3 stayed less than 5% over a much wider range than in the other two and upper limits were set arbitrarily. In order to compare these ranges and, more particularly, their lower limits*, the limiting values of ω_0 were expressed in terms of quantities which appeared to have possible significance, namely the frequencies at which M = max., M = 1 and decreasing, M = .7 and decreasing, M = .5 and decreasing, I = -max., I = -1 and decreasing in absolute value, I = -.7 and decreasing in

---

*The assumptions can be modified to increase the upper limit to any desired value.

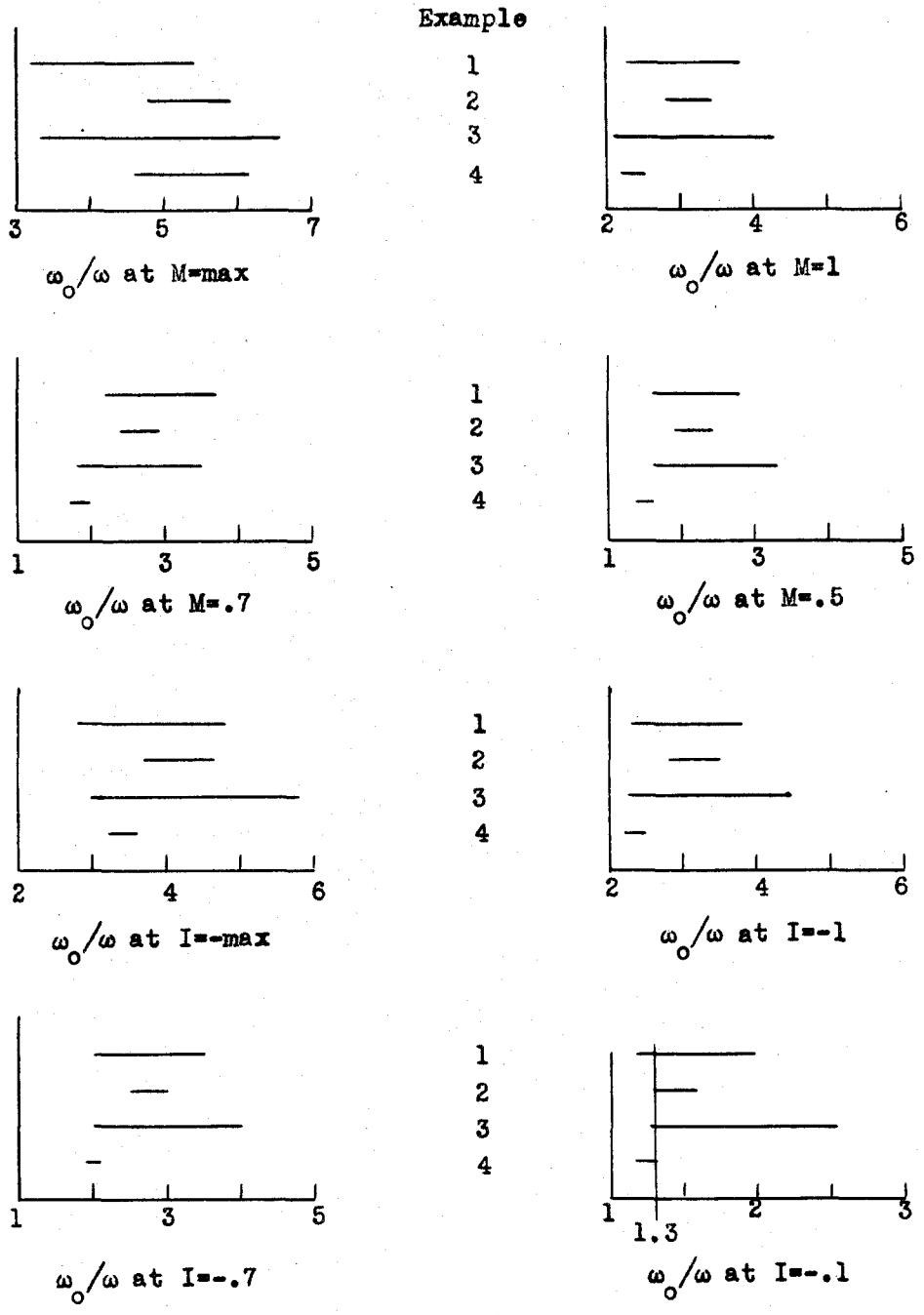

Figure 11 Satisfactory Ranges as Functions of Possibly Significant Quantities

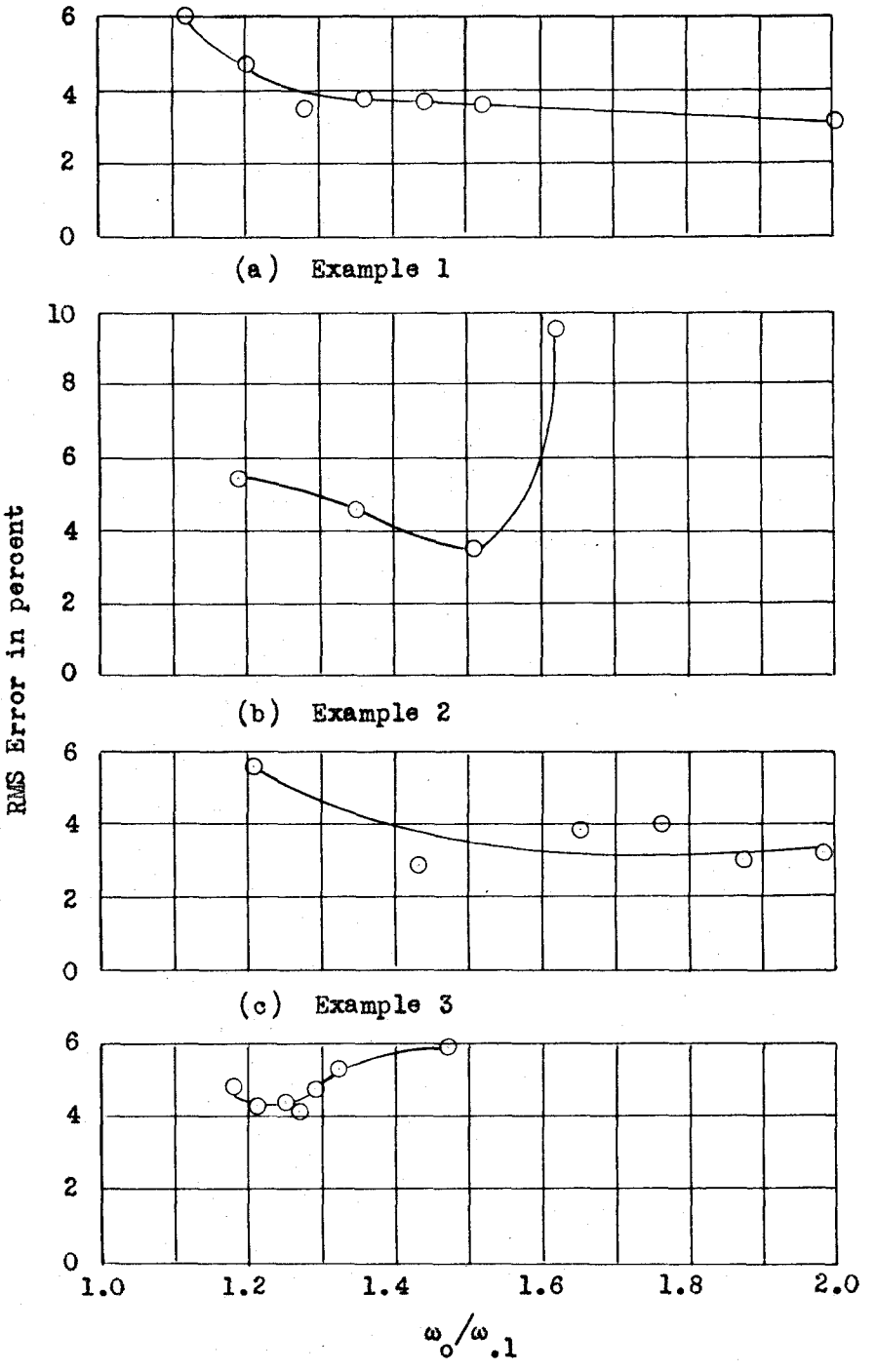

(a) Example 1

(b) Example 2

(c) Example 3

(d) Example 4

Figure 12 RMS Error vs $\omega_o/\omega_{.1}$

absolute value, and I = -.1 and decreasing in absolute value. The results of this analysis are shown in Figure 11; from these comparisons, the lower limiting values of ω_0 show the best correlation on the basis of I = -.1 and decreasing in absolute value. On this basis, ω_0 is empirically selected as equal to 1.3 times $\omega_{.1}$. In actual use, ω_0 would be selected as some convenient figure such that the ratio $\omega_0/\omega_{.1}$ would be approximately 1.3.

There are, of course, various methods of determining Fourier coefficients graphically; a method giving sufficiently accurate results for the present purpose uses graphical integration of $I(\omega) \sin n\frac{\pi}{\omega_0}\omega$ based on an eighteen interval division.

$$a_n = \frac{2}{\omega_0}\int_0^{\omega_0} I(\omega) \sin n\frac{\pi}{\omega_0}\omega \, d\omega$$

$$\sim \frac{2}{\omega_0}\sum_{k=1}^{18} I\,(2k-1)\frac{\omega_0}{36} \sin n(2k-1)5^\circ \times \frac{\omega_0}{18}$$

$$= \frac{1}{9}\sum_{k=1}^{18} I\,(2k-1)\frac{\omega_0}{36} \sin n(2k-1)5^\circ \qquad (22)$$

This choice of interval was made because of the convenient forms resulting for n = 1, 2, 3, and 4. Let $I\,(2k-1)\frac{\omega_0}{36} = I_k$, k = 1, 2, 3, ..., 18. Then

$$a_1 = \frac{1}{9}\left[(I_1+I_{18}) \sin 5^\circ + (I_2+I_{17}) \sin 15^\circ + \ldots.\right.$$

$$\left. + (I_8 + I_{11}) \sin 75^\circ + (I_9 + I_{10}) \sin 85^\circ\right] \qquad (33)$$

$$a_2 = \frac{1}{9}\Big[[(I_1+I_9) - (I_{10}+I_{18})] \sin 10^\circ + [(I_2+I_8) - (I_{11}+I_{17})] \sin 30^\circ + [(I_3+I_7) - (I_{12}+I_{16})] \sin 50^\circ + [(I_4+I_6) - (I_{13}+I_{15})] \sin 70^\circ + [I_5-I_{14}] \sin 90^\circ\Big] \quad (34)$$

$$a_3 = \frac{1}{9}\Big[(I_1+I_6-I_7-I_{12}+I_{13}+I_{18}) \sin 15^\circ + (I_2+I_5-I_8-I_{11}+I_{14}+I_{17}) \sin 45^\circ + (I_3+I_4-I_9-I_{10}+I_{15}+I_{16}) \sin 75^\circ\Big] \quad (35)$$

$$a_4 = \frac{1}{9}\Big[(I_1-I_9+I_{10}-I_{18}) \sin 20^\circ + (I_2-I_8+I_{11}-I_{17}) \sin 60^\circ + (I_3-I_7+I_{12}-I_{16}) \sin 80^\circ + (I_4-I_6+I_{13}-I_{15}) \sin 40^\circ\Big] \quad (36)$$

Only the first four terms of the series have been used in the current work both because the series convergence appears reasonably rapid and more particularly because the $h_n(t)$ terms corresponding to $n \geq 5$, if the respective Fourier coefficients are not too large, make a negligible contribution to h(t) for $\tau \leq 2\pi$ (see Figure 13). An example of this computation is given in Appendix II.

Given $I(\omega) = \sum_{n=1} a_n \sin n\frac{\pi}{\omega_0}\omega \qquad 0 \leq \omega \leq \omega_0$

$= 0 \qquad \omega > \omega_0$

and substituting in Equation (9), one obtains

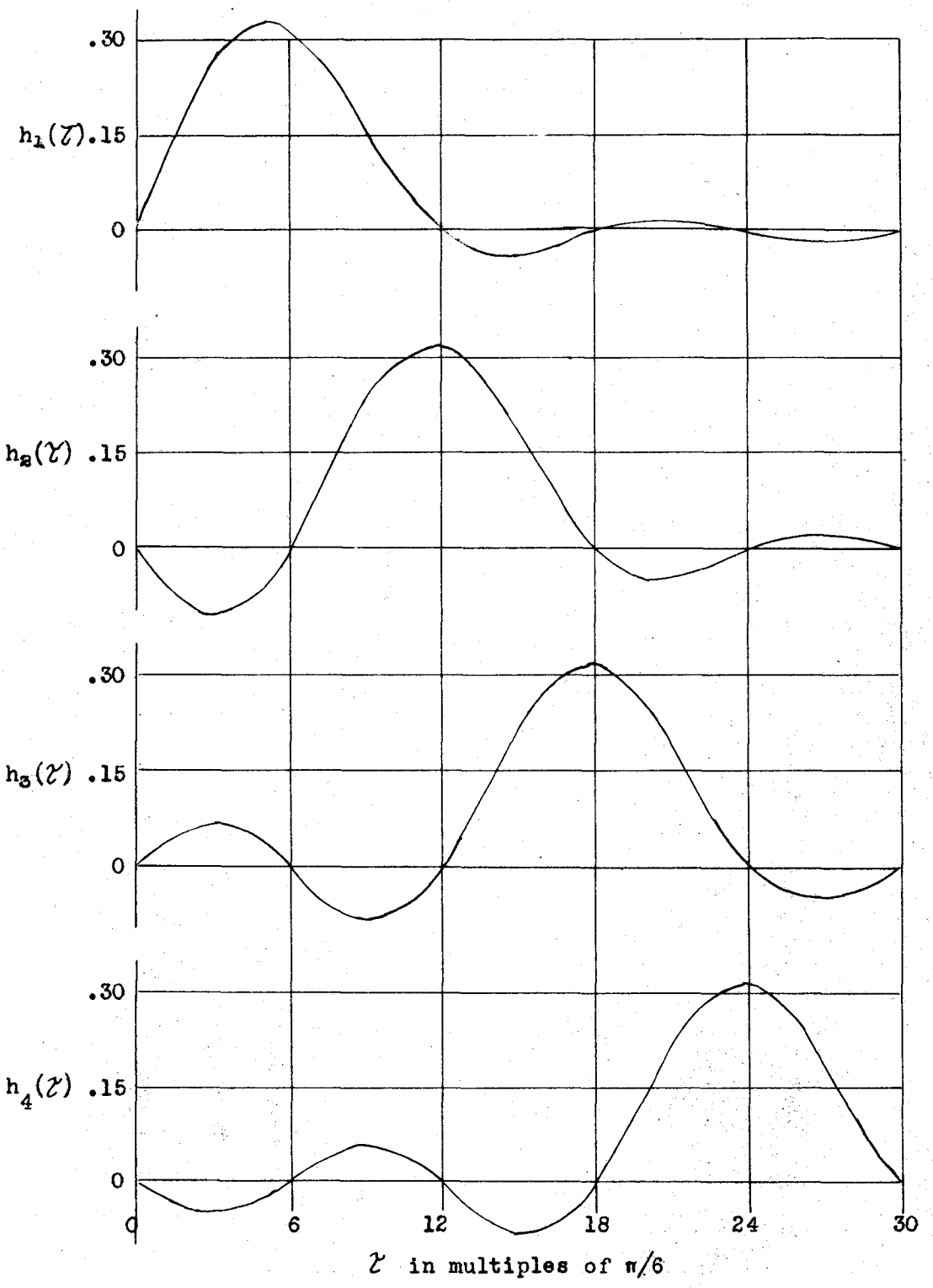

Figure 13 $h_n(\tau)$ vs τ for $\omega_o a_n = -1$

$$h(t) = -\frac{2}{\pi}\int_0^\infty I(\omega)\sin\omega t\,d\omega =$$

$$-\frac{2}{\pi}\int_0^{\omega_0}\left[\sum_{n=1}^{\infty} a_n \sin\frac{n\pi}{\omega_0}\omega\right]\sin\omega t\,d\omega$$

$$= -\frac{2}{\pi}\sum_{n=1}^{\infty}\int_0^{\omega_0} a_n \sin n\frac{\pi}{\omega_0}\omega\sin\omega t\,d\omega$$

$$= -\frac{1}{\pi}\sum_{n=1}^{\infty}\int_0^{\omega_0} a_n\left[\cos(n\frac{\pi}{\omega_0}-t)\omega - \cos(n\frac{\pi}{\omega_0}+t)\omega\right]d\omega \qquad (37)$$

since $\sin a \sin b = \frac{1}{2}\left[\cos(a-b) - \cos(a+b)\right]$.

$$h(t) = -\frac{1}{\pi}\sum_{n=1}^{\infty} a_n\left[\frac{\sin(n\frac{\pi}{\omega_0}-t)\omega}{n\frac{\pi}{\omega_0}-t} - \frac{\sin(n\frac{\pi}{\omega_0}+t)\omega}{n\frac{\pi}{\omega_0}+t}\right]_0^{\omega_0}$$

$$= -\frac{\omega_0}{\pi}\sum_{n=1} a_n\left[\frac{\sin(n\pi-\omega_0 t)}{n\pi-\omega_0 t} - \frac{\sin(n\pi+\omega_0 t)}{n\pi+\omega_0 t}\right]. \qquad (38)$$

Now, letting $\tau = \omega_0 t$ and noting that

$$\sin(n\pi-\omega_0 t) = -(-1)^n\sin\omega_0 t;\ \sin(n\pi+\omega_0 t) = +(-1)^n\sin\omega_0 t;$$

$$h(t) = -\frac{\omega_0}{\pi}\sum_{n=1}^{\infty}(-1)^n a_n\left[-\frac{\sin\tau}{n\pi-\tau} - \frac{\sin\tau}{n\pi+\tau}\right]$$

$$= \frac{\omega_0}{\pi}\sin\tau\sum_{n=1}^{\infty}(-1)^n a_n\frac{2n\pi}{n^2\pi^2-\tau^2}$$

$$= 2\omega_0\sin\tau\sum_{n=1}^{\infty}(-1)^n n\,a_n\frac{1}{n^2\pi^2-\tau^2}\ . \qquad (39)$$

The first five terms of this series are plotted individually in

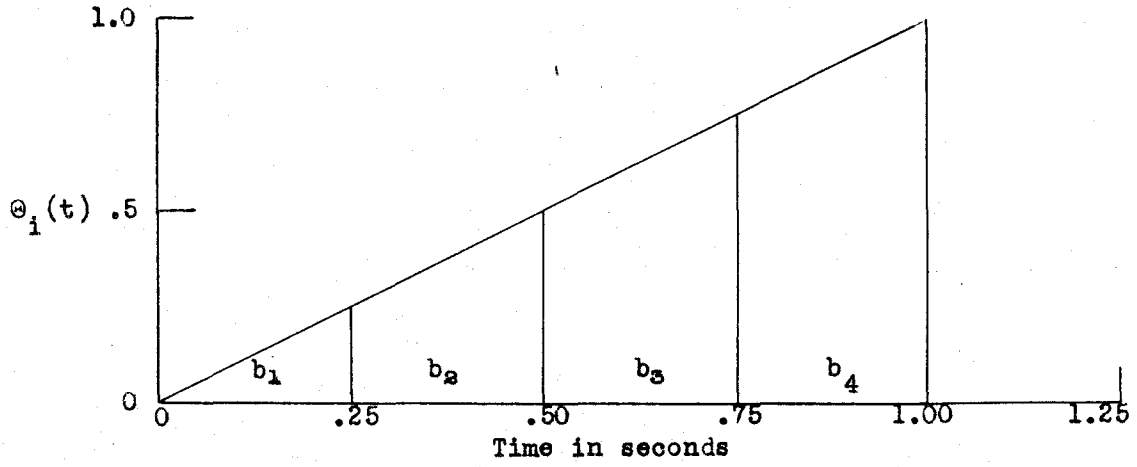

(a) $\Theta_i(t)=t$ as a Series of Impulses

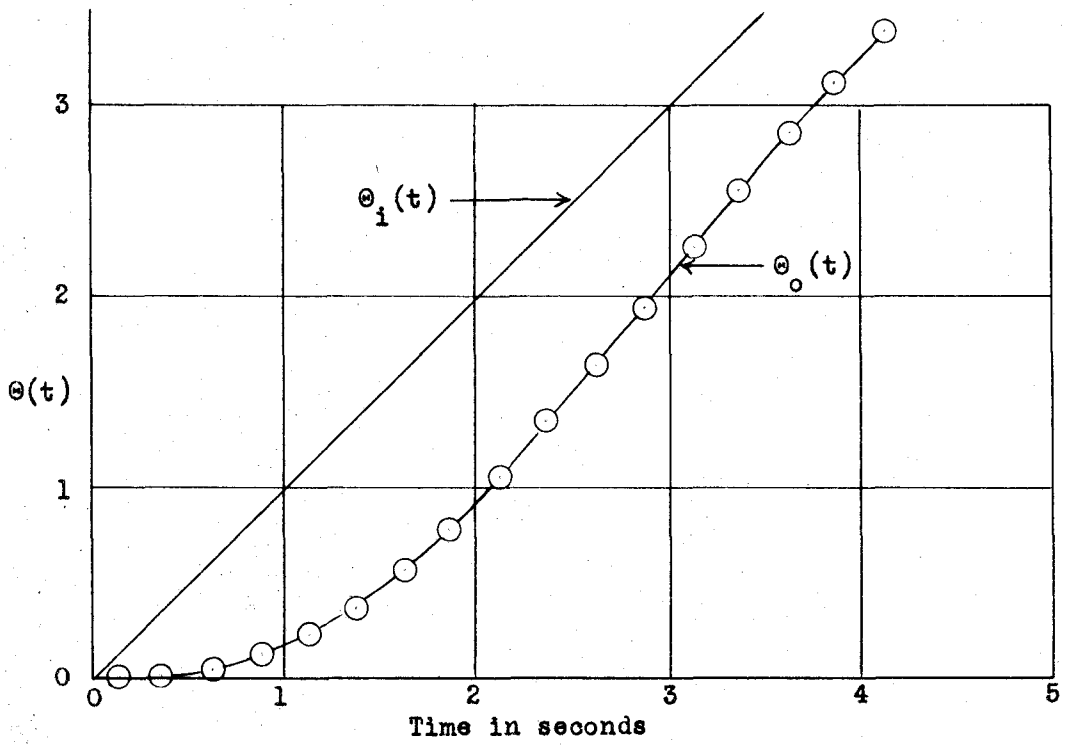

(b) $\Theta_o(t)$ and $\Theta_i(t)$ vs t for Example 1

Figure 14 Convolution Integral Approximation

Figure 13 with $\omega_o a_n = -1$. It should be noted that, for all n,

$$\lim_{\zeta \to n\pi} \frac{2n \sin \zeta}{n^2\pi^2 - \zeta^2} = \lim_{\zeta \to n\pi} \frac{2n \cos \zeta}{-2\zeta} = \frac{2n \cos n\pi}{-2n\pi}$$

$$= -\frac{(-1)^n}{\pi} = (-1)^{n+1} \times .318 \qquad (40)$$

The convolution integral, Equation (12)

$$\theta_o(t) = \int_o^t h(t-x)\, \theta_i(x)\, dx \qquad (12)$$

may be interpreted as follows: at each instant of time $x < t$, $\theta_i(x)\, dx$ represents an input impulse. The response due to this impulse contributes at a time t, a component $h(t-x)\, \theta_i(x)\, dx$. The total response at time t is then the sum or integral over the range 0 to t of these individual components. Methods of approximating this integral are given by Floyd[9] and Tustin[11]. The latter has been used in Appendix III to derive the results given in Figure 14.

EXAMPLES

Four systems have been studied in this investigation. These examples were chosen to have a variety of $KG(\omega)$ characteristics but were kept simple enough so that the roots of the characteristic equations could be found with reasonable accuracy by analytical methods. No dimensions were assigned to the input and output quantities of these systems since the only physical restriction present is that both input and output have the same dimensions. The symbolism θ_i and θ_o indicates angular position control systems but this is merely a heritage from the early theoretical work.

Figures 15 to 21 are included to show the types of agreement between the predicted and actual impulse responses in the examples. Since these two curves differ only slightly in most cases, attempting to show both on a single plot seemed inadvisable. Therefore, in all h(t) curves herein, the continuous line represents h(t) as computed from the system characteristic equation and the circles show points predicted by the method proposed in the preceding section. Figures 16, 18, 19, and 21 are for values of $\omega_o/\omega_{.1}$ near the empirically chosen 1.3; Figures 15 and 20 are for lower values of this ratio and Figure 17 for a higher value. The $KG(\omega)$ information for Examples 1 and 4 is shown in the preceding Figures 4 and 8, the derived curves of $I(\omega)$ vs ω being Figures 5 and 9. The expressions for $KG(\omega)$, $H(s)$,

and h(t) for the four examples are given below.

Example 1

$$KG(\omega) = \frac{1.36}{j\omega(1+j\omega)} \tag{41}$$

$$H(s) = \frac{1.36}{s^2+s+1.36} = 1.29 \ \frac{1.053}{(s+.5)^2+(1.053)^2} \tag{42}$$

$$h(t) = 1.29\, e^{-.5t} \sin 1.053t \tag{43}$$

Example 2

$$KG(\omega) = \frac{.118(1+j6\omega)}{-\omega^2(1+j\omega)} \tag{44}$$

$$H(s) = \frac{.118(1+6s)}{s^3+s^2+.708s+.118} = \frac{-.0915}{s+.22}$$

$$+ \frac{.585 \angle -85.55}{s+.39-j.62} + \frac{.585 \angle +85.55}{s+.39+j.62} \tag{45}$$

$$h(t) = -.0915e^{-.22t} + 1.17e^{-.39t} \sin(.62t + 4.45^\circ) \tag{46}$$

Example 3

$$KG(\omega) = \frac{20.6(1+j.5\omega)}{j\omega(1+j.125\omega)(1+j\omega)} \tag{47}$$

$$H(s) = \frac{164.8(1+.5s)}{s^3+9s^2+90.4s+164.8} = \frac{-.227}{s+2.18}$$

$$+ \frac{5.17\angle -88.75}{s+3.41-j7.98} + \frac{5.17\angle +88.75}{s+3.41+j7.98} \tag{48}$$

$$h(t) = -.227e^{-2.18t} + 10.34e^{-3.41t}\sin(7.98t + 1.25^\circ) \tag{49}$$

Example 4

$$KG(\omega) = \frac{5(1+j\omega)^2}{(j\omega)^2(1+j.05\omega)^2} \tag{50}$$

$$H(s) = \frac{5(1+s)^2}{.0025s^5+.15^4+s^3+5s^2+10s+5}$$

$$= \frac{.09}{s+.726} + \frac{-6.36}{s+2.8} + \frac{3.58}{s+28.13} + \frac{11.38\angle -83.2}{s+4.17-j4.18}$$

$$+ \frac{11.38\angle +83.2}{s+4.17+j4.18} \tag{51}$$

$$h(t) = .09e^{-.726t} - 6.36e^{-2.8t} + 3.58e^{-28.13t}$$

$$+ 22.76e^{-4.17t}\sin(4.18t + 6.8^\circ) \tag{52}$$

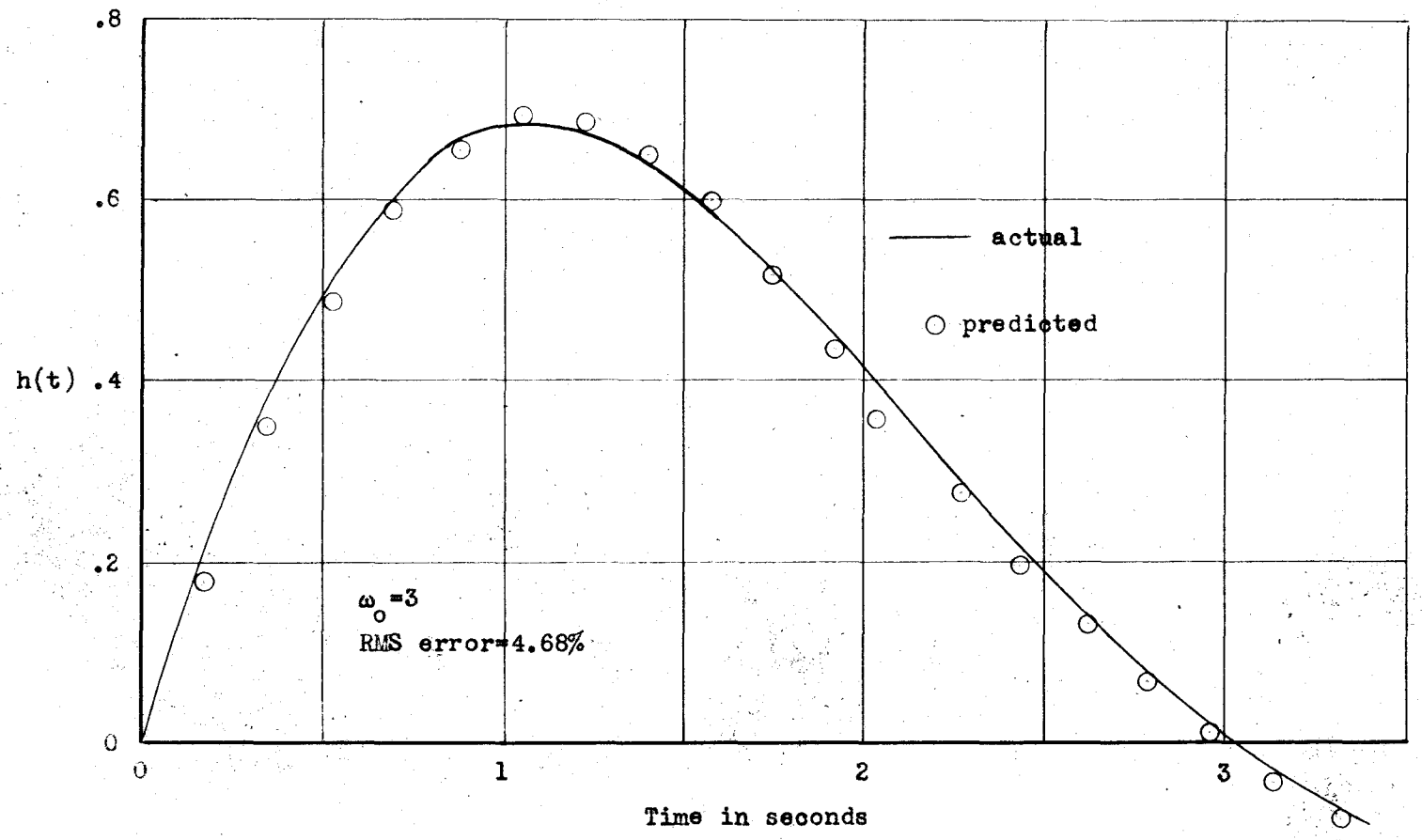

Figure 15 h(t) vs t, Example 1, $\omega_o/\omega_{.1}$=1.20

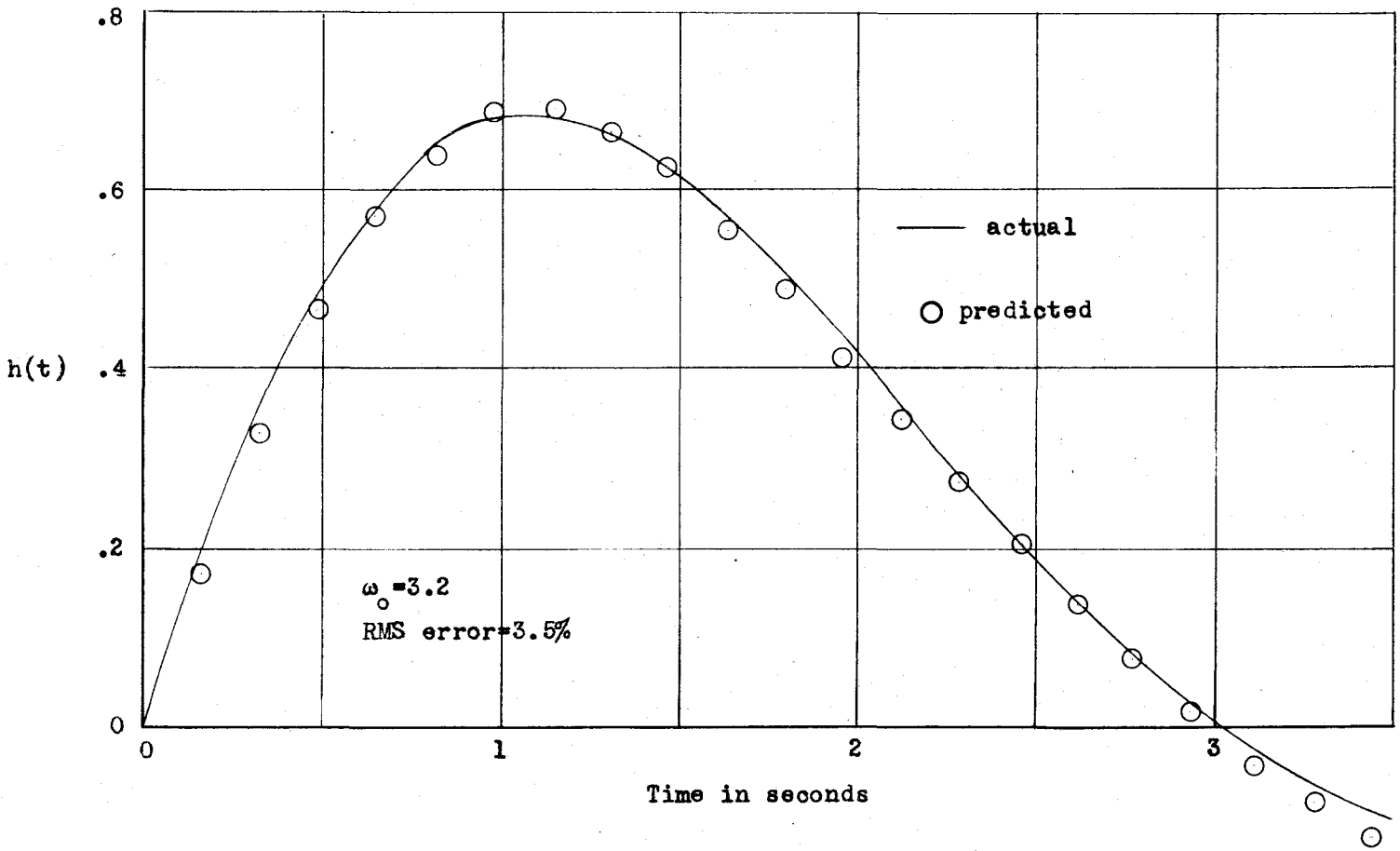

Figure 16 h(t) vs t, Example 1, $\omega_o/\omega_{.1}$=1.28

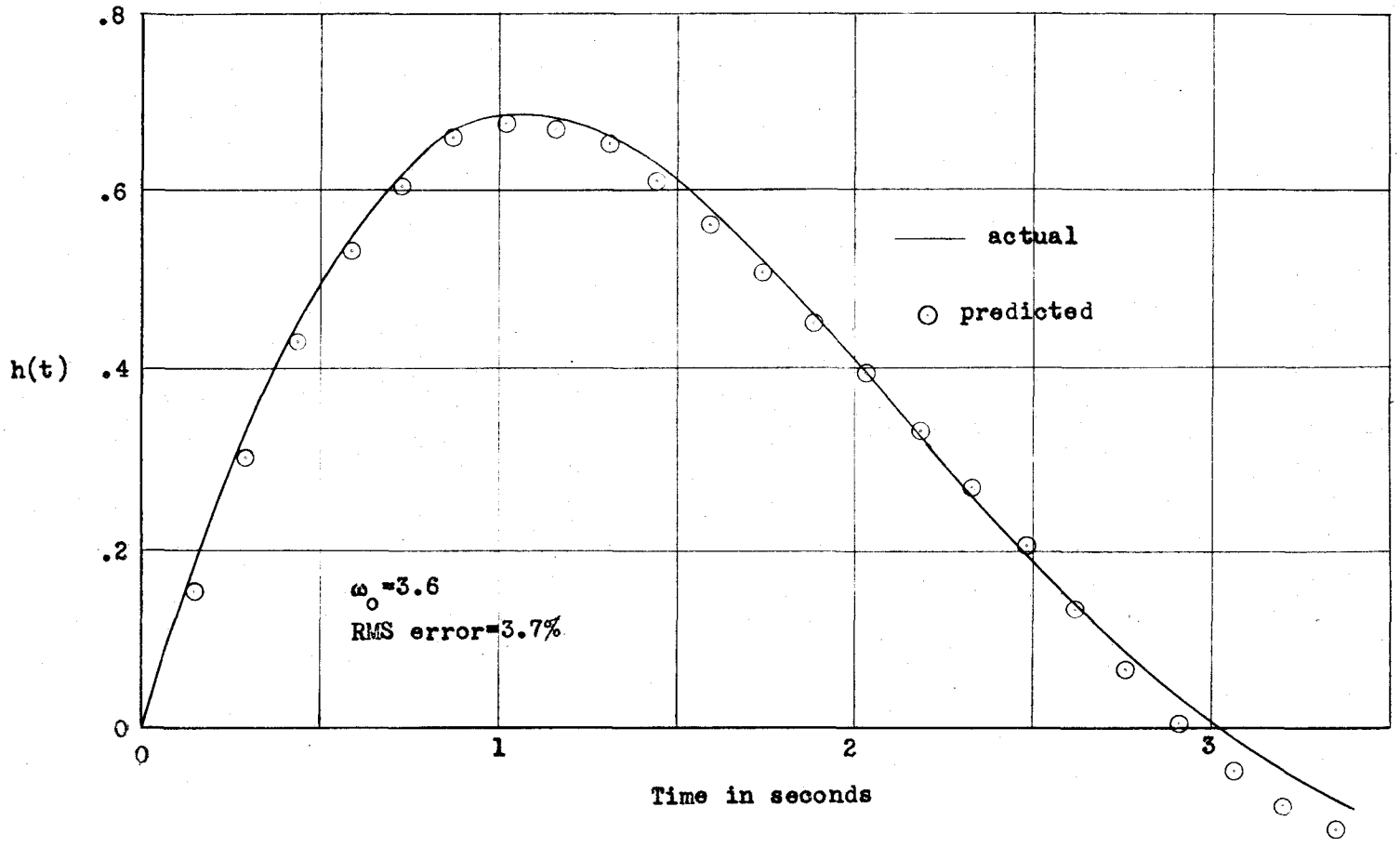

Figure 17 h(t) vs t, Example 1, $\omega_o/\omega_{.1}$=1.44

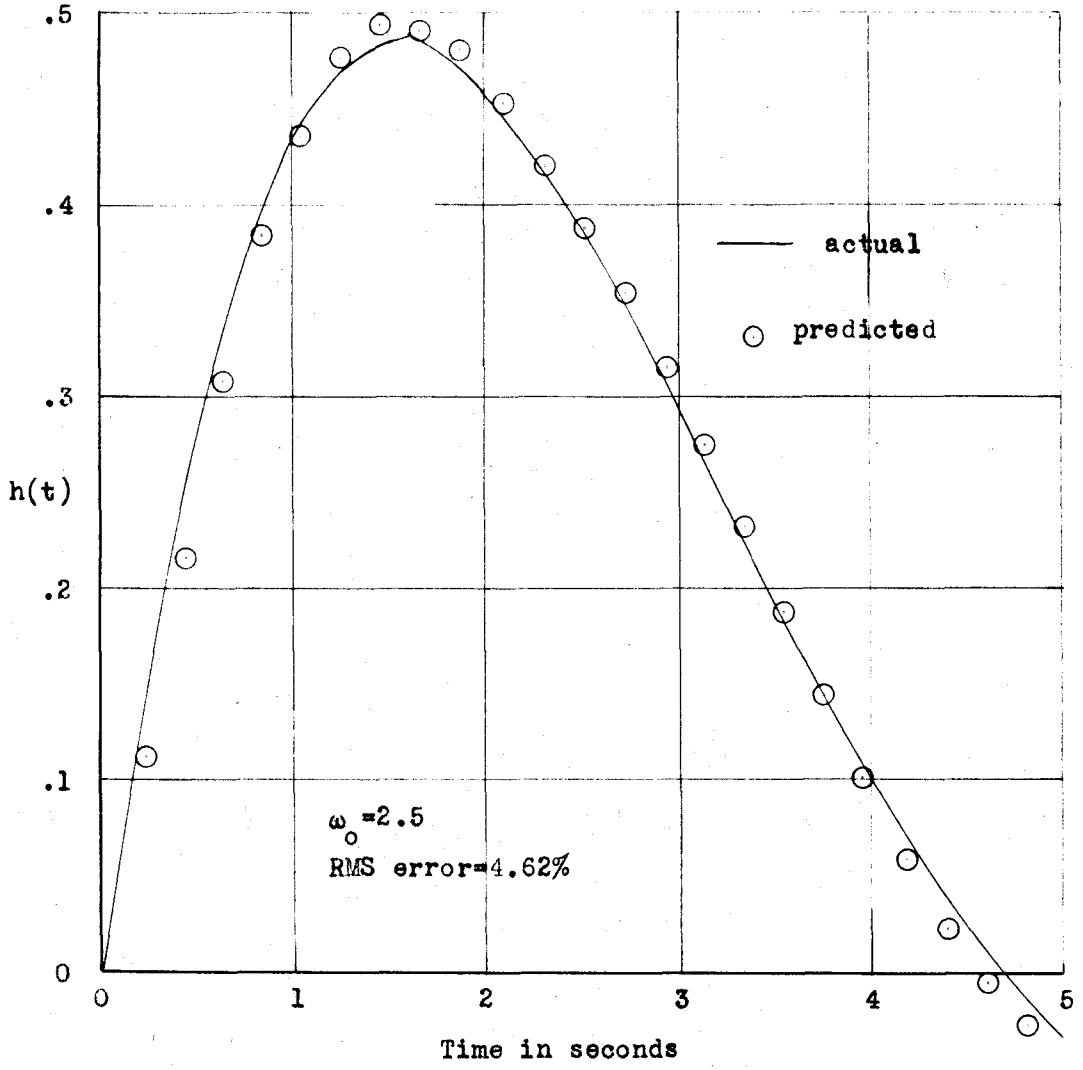

Figure 18 h(t) vs t, Example 2, $\omega_o/\omega_{.1}$=1.35

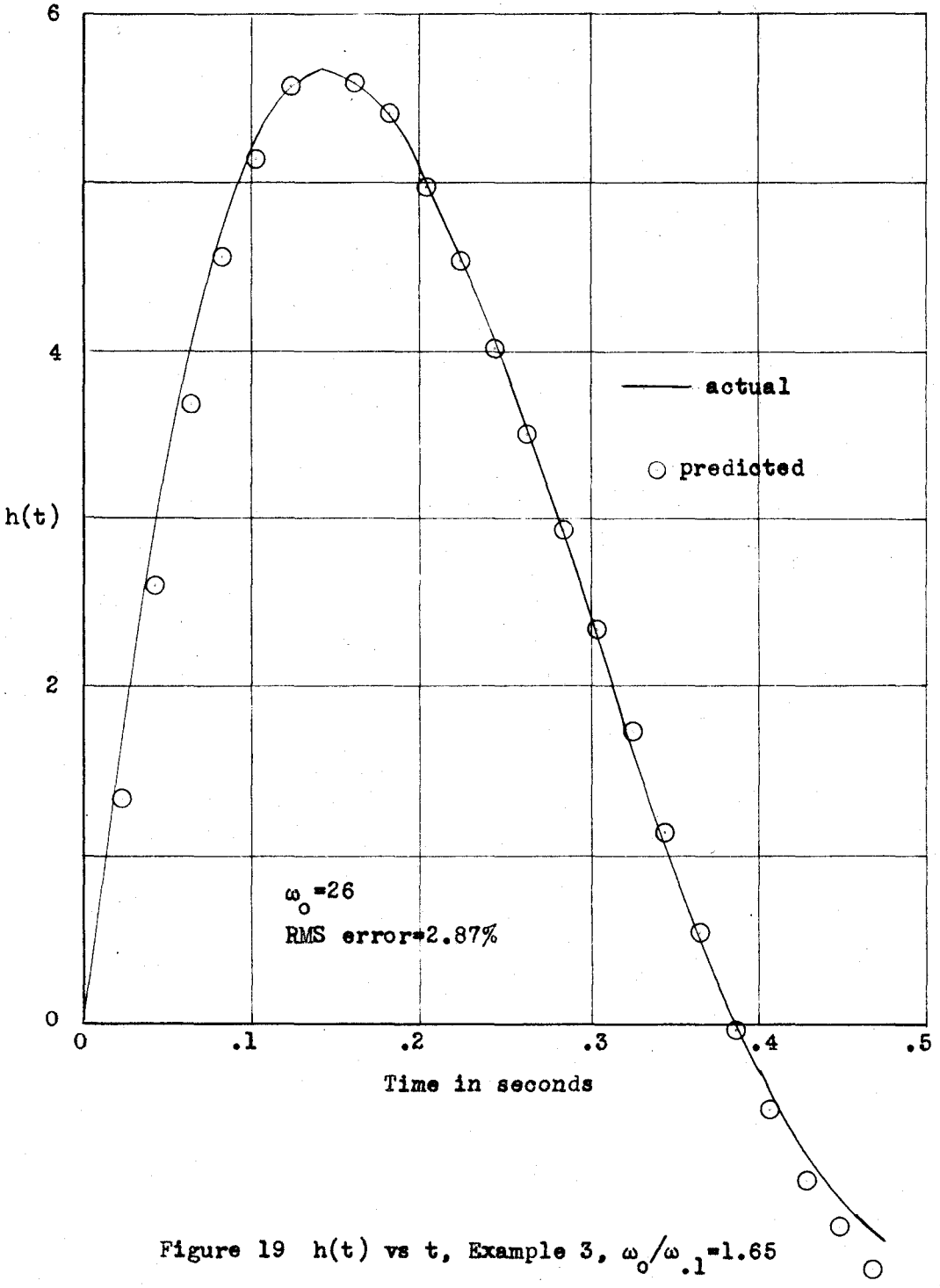

Figure 19 h(t) vs t, Example 3, $\omega_o/\omega_{.1}$=1.65

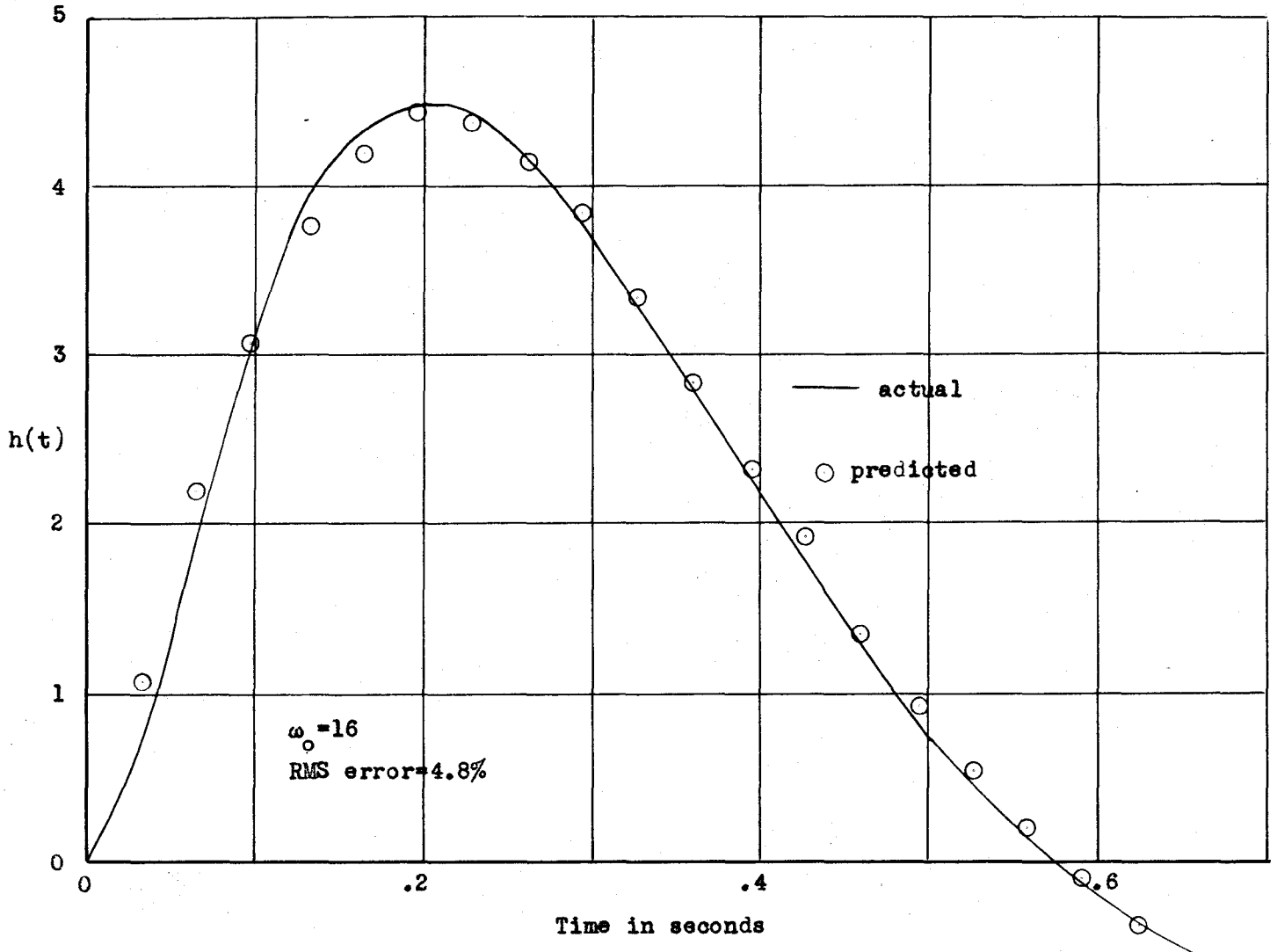

Figure 20 h(t) vs t, Example 4, $\omega_o/\omega_{.1}$=1.18

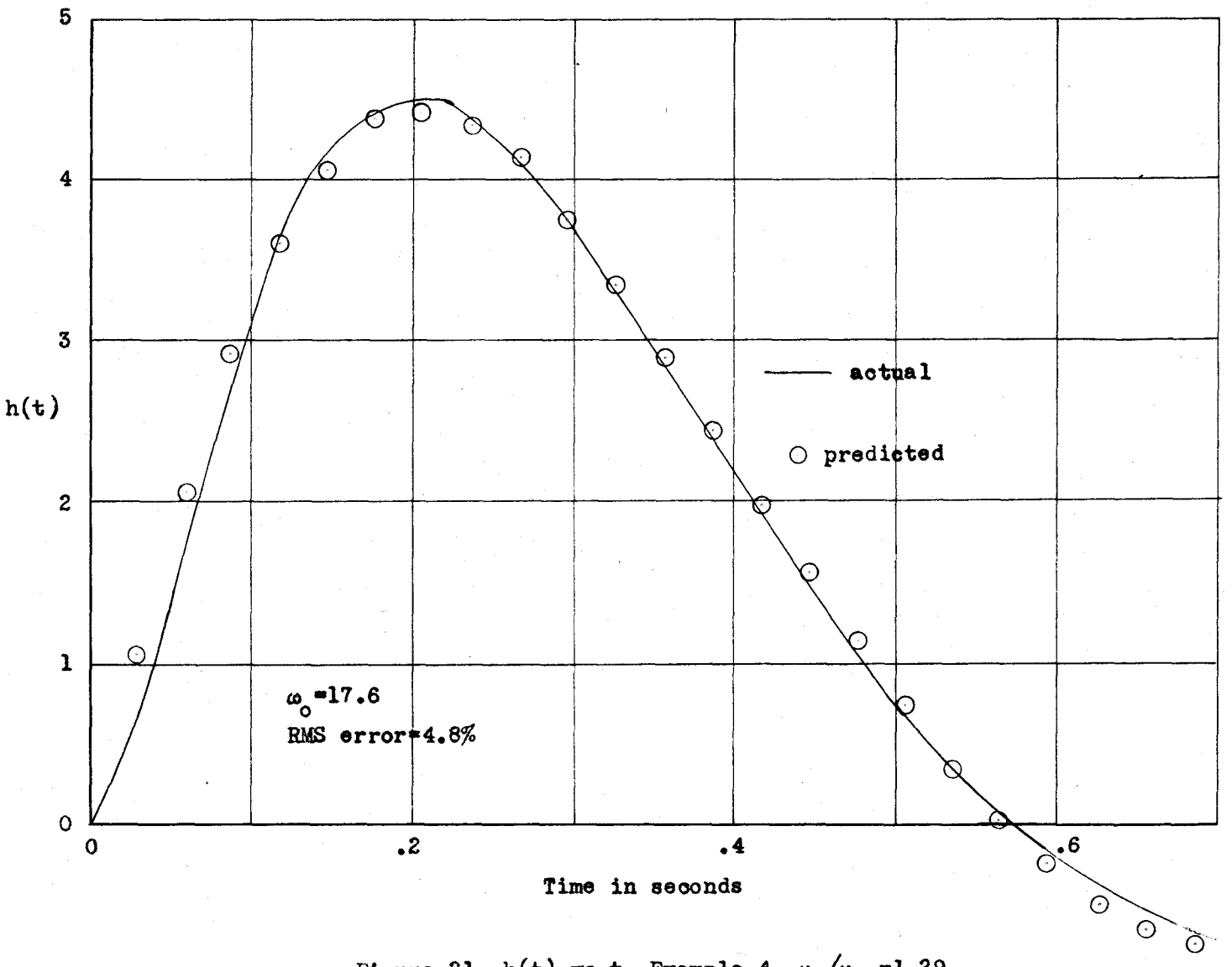

Figure 21 h(t) vs t, Example 4, $\omega_o/\omega_{.1}$=1.29

DISCUSSION

The differences between the Fourier coefficients, a_n, obtained by eighteen point graphical integration and those giving exact agreements with h(t) at the $\tau = n\pi$ points vary as ω_0 is changed. As ω_0 starts from low values, poor agreement results since an appreciable part of $I(\omega)$ is being neglected (see Figure 10). As ω_0 increases, the differences decrease and might be expected to remain small. However, since a fixed number of points are used in the graphical integration, the spacing between points increases with ω_0 and the detail of the $I(\omega)$ curve may be lost. This loss of detail may affect the values obtained for the a_ns in a quite random manner. To consider an extreme example (Figure 22), suppose $I(\omega)$ consists of a single narrow triangular pulse. As ω_0 increases, an integration point may fall on the peak of the pulse, part way up either side, or at very large ω_0, may miss the pulse entirely, resulting in a wide range of coefficient values for relatively small changes in ω_0.

Any physical servomechanism will give rise to a curve of $I(\omega)$ vs ω which decreases rapidly with increasing frequency beyond ω_{-3}. $I(\omega) = \mathcal{I} H(\omega) = \mathcal{I} \frac{KG(\omega)}{1+KG(\omega)}$. Now, for the higher frequencies being considered, practically all the time constants of the system have become effective and $KG(\omega)$ is decreasing at a rate equal to or greater than twelve decibels per octave. Further, the angle of $KG(\omega)$ is near 180° and

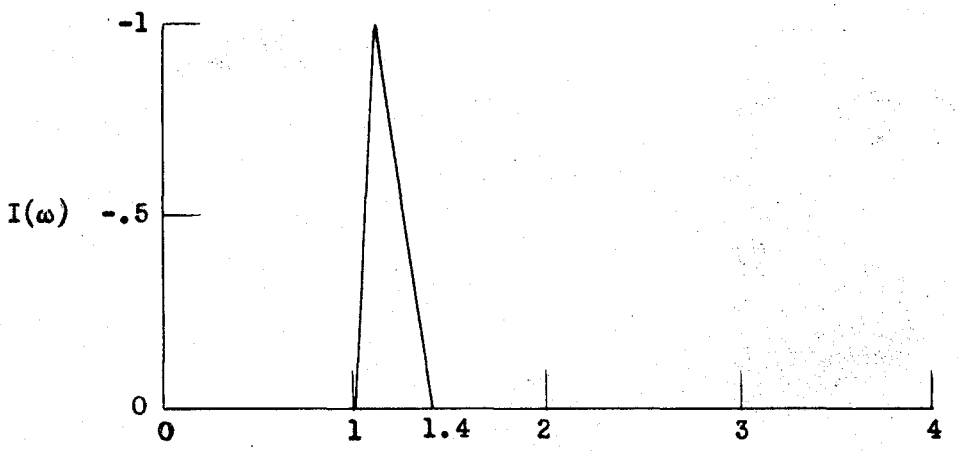

ω_o	Integration Points
3.60	.1, .3, .5, .7, .9, 1.1, 1.3, 1.5
4.50	.125, .375, .625, .875, 1.125, 1.375, 1.500
5.40	.15, .45, .75, 1.05, 1.35, 1.65
7.20	.2, .6, 1.0, 1.4, 1.8
7.92	.22, .66, 1.10, 1.54
9.00	.25, .75, 1.25, 1.75

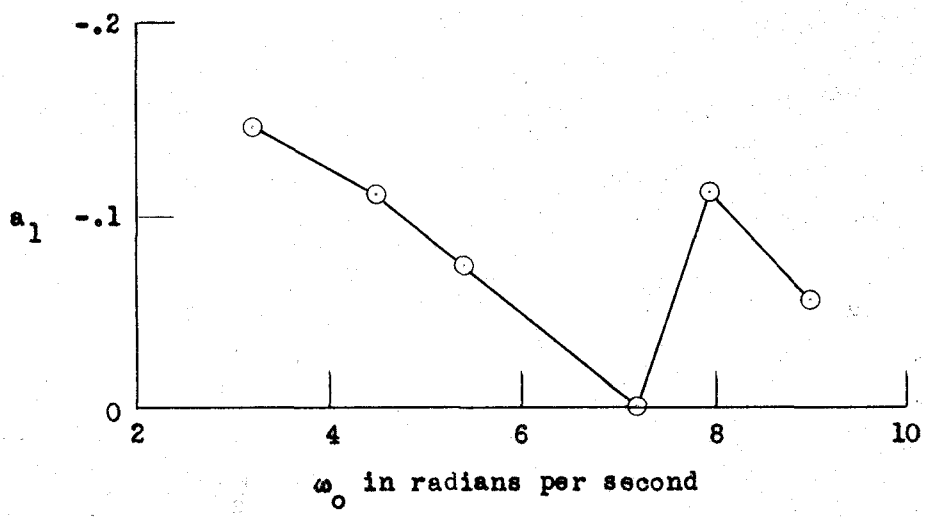

Figure 22 Loss of Detail with Increasing ω_o

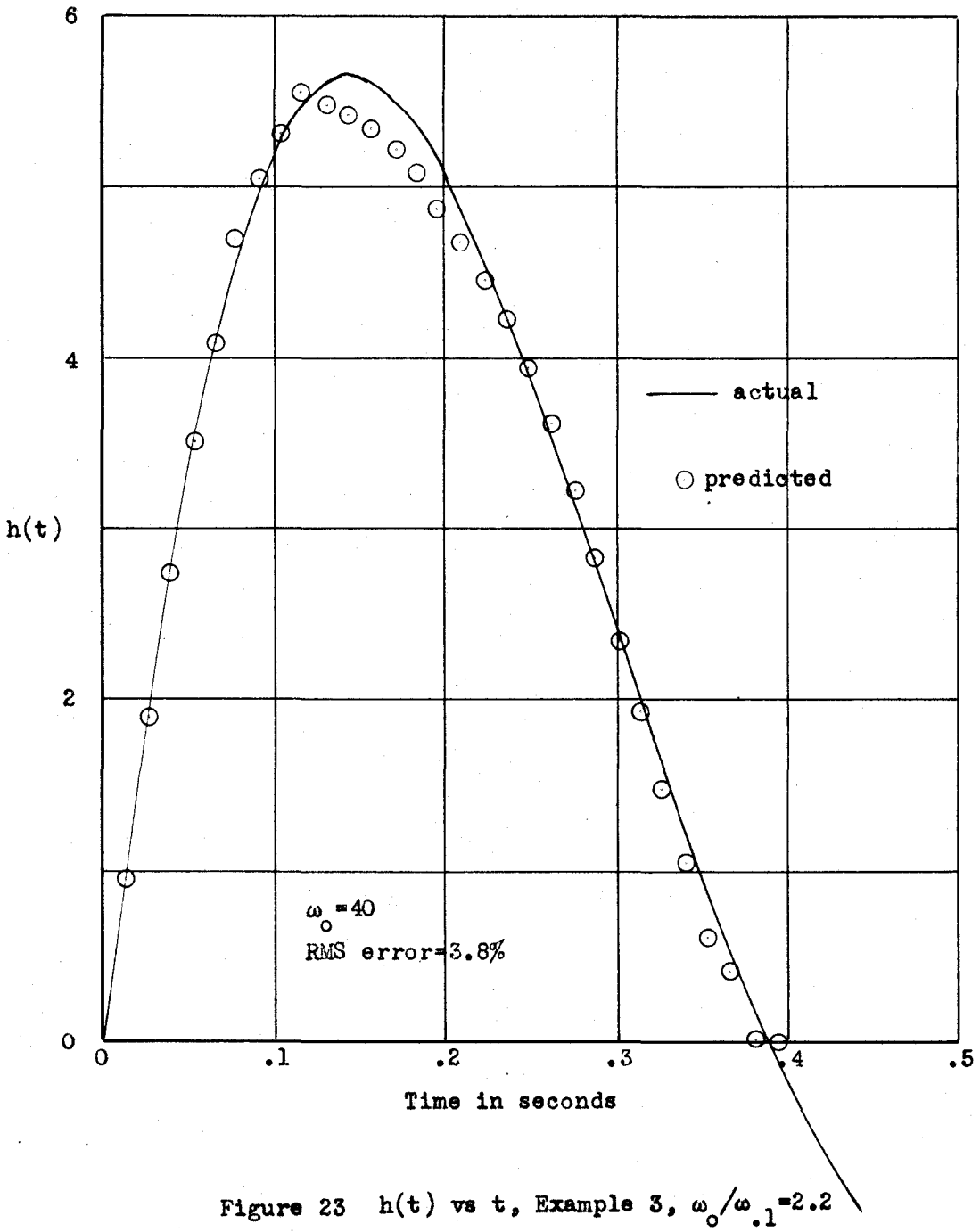

Figure 23 h(t) vs t, Example 3, $\omega_o/\omega_{.1}$=2.2

hence stability requires that $KG(\omega)$ be small. Under these conditions $1 + KG(\omega)$ is approximately 1 and therefore $H(\omega)$ is approximately equal to $KG(\omega)$. But $I(\omega)$ is only one component of $H(\omega)$ and must therefore also be decreasing at a rate of at least twelve decibels per octave.

For values of I less than .1, the loci radius 1/2I becomes very large and hence these loci are not easily drawn; for this reason and because the contribution of $I(\omega)$ between $\omega_{.1}$ and ω_0 would in any case be small, the Fourier coefficients were computed under the assumption that $I(\omega)$ was linearly decreasing between $\omega_{.1}$ and ω_0. This assumption was valid, as shown by the $\tau = n\pi$ point agreements in the cases investigated except in Example 3 when ω_0 was taken equal to 40 radians per second (Figure 23). Since $\omega_{.1}$ was only 18.2 radians per second, many of the integration points fell in the range where the behavior of $I(\omega)$ was assumed rather than known and led to a value for a_8 of -421 whereas -440 was the value necessary to give agreement at $\tau = 2\pi$. Since $\omega_0 > 2\omega_{.1}$, all the points on the assumed tail acted to decrease a_8. However, even in this extreme example, the RMS error was acceptable and the values of the other coefficients were not appreciably affected. The same difficulties exist in determining the behavior of $I(\omega)$ below the frequency where $I(\omega) = -.1$ and is increasing. However, this is a small, known frequency range and will make a very small contribution to the coefficient values.

If the terms retained in the series for $I(\omega)$ do not include all those of appreciable size, the existence of those omitted appears in the predicted curve as an almost sinusoidal effect with nodes at

$t = \frac{n\pi}{\omega_0}$. The difference between the predicted and computed h(t)s for Example 4 with $\omega_0 = 20$ is plotted in Figure 24 and clearly shows this effect. This curve, together with all other plots of Example 4, shows that the computed value of h(t) for times less than one tenth of a second is lower than the predicted value. This is believed to result from insufficient precision in determining the roots of the fifth order equation of Example 5 leading to too large a coefficient for the $e^{-2.8t}$ term in Equation (52).

It is not, however, true that the neglected terms must be very small but only that their contributions at the times considered be small. Figure 25 illustrates this for the case of Example 3 with $\omega_0 = 52$. In this figure the $I(\omega)$ actually used in the computation (four terms) is plotted on the same axes as the true $I(\omega)$. Despite the large difference between these curves, the RMS error was only 3.96%.

Since the $h_n(t)$ terms were not plotted individually but were summed at $\gamma = \frac{\pi}{6}$ intervals, there is no assurance that the largest value so obtained is actually the peak value of h(t); however, the curve is known to be continuous and for all $\omega_0 > \omega_{.1}$ in the examples considered, the interval $\gamma = \frac{\pi}{6}$ was found to be sufficiently small to leave little doubt as to the shape of h(t) between computed points. Should these points be too far apart for satisfactory plotting in a particular case, Equation (39) can be used to determine points intermediate between those tabulated on the computation form in Appendix II.

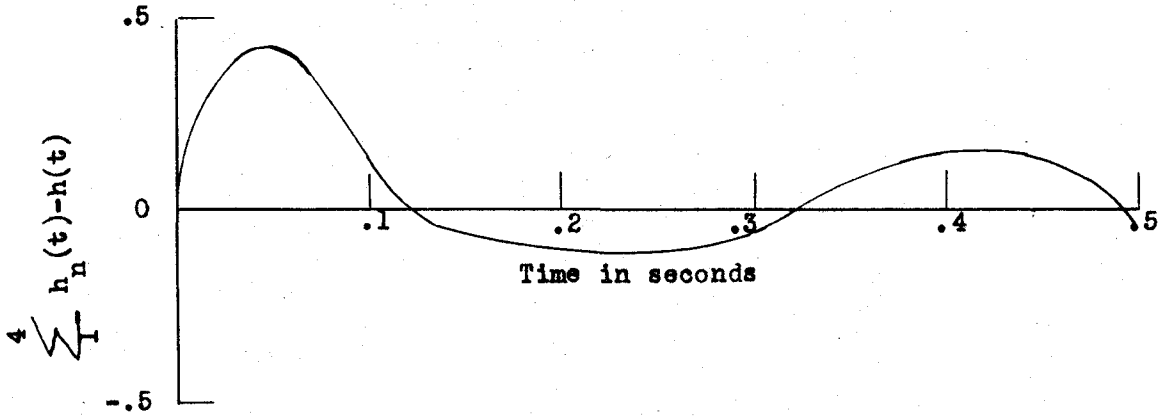

Figure 24 Difference between Predicted and Computed h(t)s for Example 4 with ω_o=20

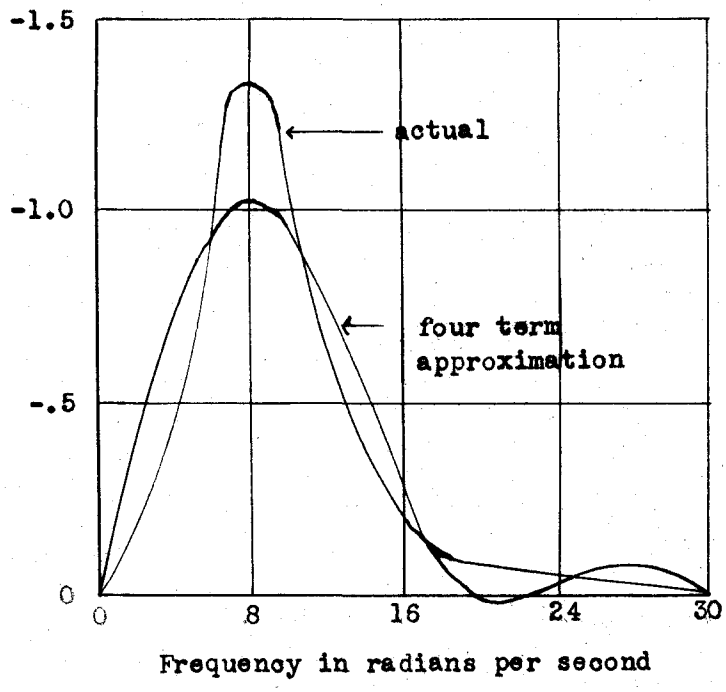

Figure 25 Comparison of True and Approximate I(ω) for Example 3 with ω_o=32

Since only a few terms of the Fourier series for $I(\omega)$ are to be retained, it would appear that a method of determining coefficients such as the Fischer-Hinnen procedure might be applicable since they involve much less labor than graphical integration. However, such methods require the assumption that all coefficients of higher order are zero; since this assumption is not generally justified, these methods would lead to erroneous values of a_1, a_2, a_3 and a_4 giving invalid $h(t)$ curves. Hence a method must be used which does not assume that the neglected coefficients are zero.

In the earlier stages of this investigation, belief that a good approximation to $I(\omega)$ by four terms of the Fourier series would be desirable and that great accuracy in the coefficient determination would be unnecessary led the author to development of an electronic harmonic generator which produced in-phase sine waves of four, eight, twelve, and sixteen kilocycles whose magnitudes and signs were individually controllable. The output of this device was fed to a cathode ray oscilloscope over whose screen was fastened a plot of $I(\omega)$ vs ω on transparent paper. The cutoff frequency, ω_0, was adjusted by varying the horizontal gain of the oscilloscope and the component magnitudes varied to give a good visual fit between the true curve and the sum of the four components. Satisfactory data could not be obtained due to the low accuracy with which the magnitudes could be read and for the reason stated in the preceding paragraph.

CONCLUSIONS

The proposed method meets its objectives in giving excellent agreement between actual and predicted impulse responses with a relatively small amount of computation. Use of forms such as those of Appendix II reduces the necessary computation to the routine level once the curve of $I(\omega)$ vs ω is available.

Since the effect of terms higher than the fourth in the expansion for $h(t)$ is very small for $t < \frac{\pi}{\omega_0}$ and quite small for $t < \frac{2\pi}{\omega_0}$, the initial rate of rise of $h(t)$ is accurately predicted in all examples. Further this method gives very close agreement on maximum values, the time of the maximum, and the time when $h(t)$ decreases to zero. $h(t)$ is, of course, not to be predicted by this method beyond $t = \frac{n\pi}{\omega_0}$ where n is the number of terms retained in the Fourier representation of $I(\omega)$. For instance, if only four terms are retained, the predicted value of $h(\frac{5\pi}{\omega_0})$ will be zero regardless of its proper value. However, unless a_5 and higher terms are comparatively very large, good agreement is to be expected in the range $0 < t < \frac{4\pi}{\omega_0}$.

The manipulation of $KG(\omega)$ to obtain $I(\omega)$ and the determination of the Fourier coefficients, both as to magnitude and sign, must be done with considerable care to obtain valid $h(t)$ curves.

Where the designer does not have other more important considerations, the use of the Nyquist presentation rather than the lm-ang

presentation is recommended due to the much greater ease of plotting the loci of constant I and due to the fact that the lm-ang plot tends to concentrate the region of interest in a much smaller area.

All of the examples chosen involve only series connections of system components with direct unity feedback so that $\frac{\theta_o}{\mathcal{E}} = KG$ actually exists in the system. To apply the method to more complicated systems, having minor feedback loops or elements in the main feedback path, KG could still be determined as $\frac{\theta_o}{\theta_i - \theta_o}$. Unless $I(\omega)$ should in such a case have a shape completely different from those considered, such as two peaks or a single much wider peak, there is no reason to suppose that the proposed method is inapplicable.

RECOMMENDATIONS

The following matters might profitably be the subject of further investigation:

1. The best general assumption on the behavior of $I(\omega)$ between $\omega_{.1}$ and ω_0.
2. Additional examples of more complex systems using an analog computer to determine the actual response.
3. The expansion of a given $h(t)$ into a series of the form used herein leading to the required frequency response corresponding to a given time response, i.e. the reverse process.
4. The approximation of $I(\omega)$ by sinusoidal terms not of the same period and having various numbers of half cycles before cutoff.

LITERATURE CITED

1. American Institute of Electrical Engineers Committee Report. Proposed Symbols and Terms for Feedback Control Systems. Electrical Engineering. Vol. 70. Pages 905-909. October. 1951.

2. Brown, G. S. and Campbell, D. P. Principles of Servomechanisms. N. Y., John Wiley and Sons, Inc. 1948.

3. Nyquist, H. Regeneration Theory. Bell System Technical Journal. Vol. 11. Pages 126-147. January. 1932.

4. Bode, H. W. Network Analysis and Feedback Amplifier Design. N. Y., D. Van Nostrand Co. 1945.

5. Bedford, A. V. and Fredendall, G. L. Transient Response of Multistage Video-Frequency Amplifiers. Proceedings of the Institute of Radio Engineers. Vol. 27. Pages 277-284. April. 1939.

6. Chestnut, H. and Mayer, R. W. Servomechanisms and Regulating System Design. Vol. 1. N. Y., John Wiley and Sons, Inc. 1951.

7. Harris, H. Jr., Kirby, M. J., and von Arx, E. F. Servomechanism Transient Performance from Decibel-Log Frequency Plots. American Institute of Electrical Engineers Transactions. Vol. 70. Section T 1-269. 1951.

8. Wheeler, H. A. The Interpretation of Amplitude and Phase Distortion in Terms of Paired Echoes. Proceedings of the Institute of Radio Engineers. Vol. 27. Pages 359-384. June. 1939.

9. Floyd, G. F. Method for Approximating the Transient Response from the Frequency Response. In Brown, G. S. and Campbell, D. P. Principles of Servomechanisms. N. Y., John Wiley and Sons, Inc. 1948.

10. Bedford, A. V. and Fredendall, G. L. Transient Response of Television Amplifiers. Proceedings of the Institute of Radio Engineers. Vol. 30. Pages 440-457. October. 1942.

11. Tustin, A. Method of Analyzing Behavior of Linear Systems in Terms of Time Series. Journal of the Institute of Electrical Engineers. Vol. 94. Part II-A. Pages 130-142. 1947.

APPENDICES

APPENDIX I

The symbols associated with time and frequency response of servomechanisms are shown in Figure 26. The first three parts of this figure stress the feedback concept for the cases where the input is a unit impulse, an arbitrary function of time, and a unit sinusoid. The fourth part introduces the symbols used when the system is considered in terms of its input and output without regard to the internal arrangement.

The A. I. E. E. Committee[1] has proposed definitions for two of these quantities:

> The controlled variable (Θ_o) is that quantity or condition of the controlled system which is directly measured and controlled.
>
> The command (Θ_i) is the input which is established or varied by some means external to and independent of the feedback control system under consideration.

No dimensions have been expressed or implied for input, output, or error. Since the systems considered have direct unity feedback, the only requirement is that these three quantities all have the same dimensions; this is also the condition needed to make $KG(\omega)$ and $H(\omega)$ dimensionless as they must be.

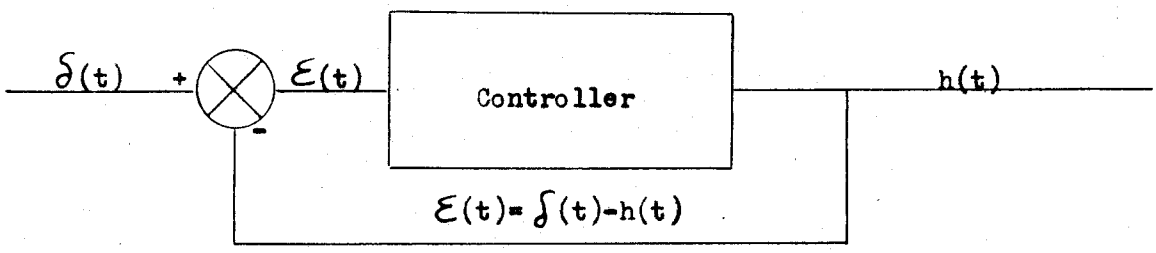

(a) Unit Impulse Input, $\Theta_i(t) = \delta(t)$

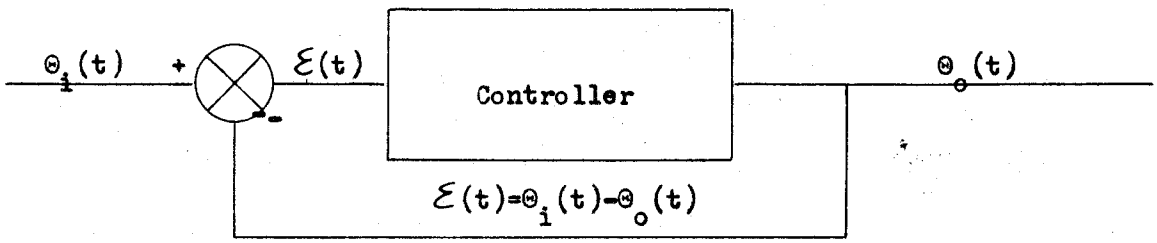

(b) Arbitrary Time Function Input, $\Theta_i(t) = f(t)$

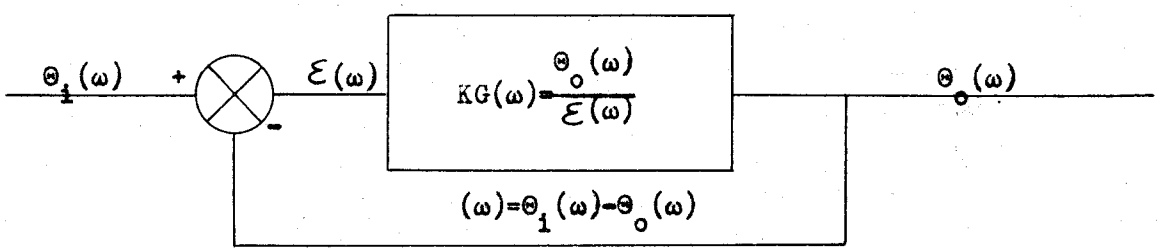

(c) Sinusoidal Input, $\Theta_i(\omega) = 1+j0$

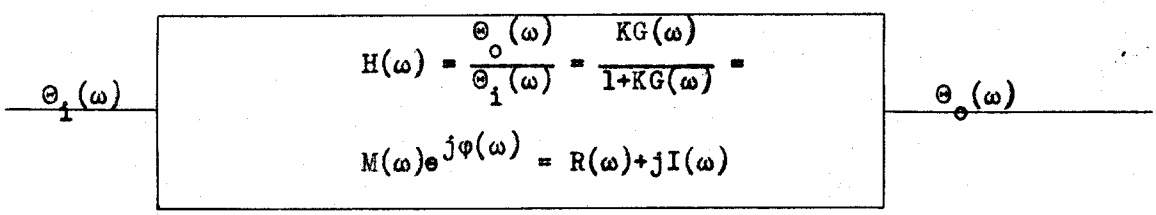

(d) Sinusoidal Input, $\Theta_i(\omega) = 1+j0$

Figure 26 Symbolism

APPENDIX II

No special merit is claimed for the following forms which are similar to those actually used in this investigation. However, it should be noted that a high degree of symmetry exists in the forms for a_1 and a_2 and that the forms for a_3 and a_4 can be filled out in a cyclic manner. The use of a colored pencil for negative quantities was found to improve speed and accuracy.

The data for $h_n(t)$, n = 1, 2, 3 and 4, can be abstracted and put in any other form more suitable for a particular investigation. Similar data for n = 5 is included below.

Table 1

$h_5(\tau)$ for $\tau = n\pi/6$; $\omega_0 a_5 = -1$

n	$h_5(\tau)$	n	$h_5(\tau)$	n	$h_5(\tau)$
1	.020	11	-.023	21	-.079
2	.035	12	.000	22	-.076
3	.041	13	.025	23	-.049
4	.036	14	.045	24	.000
5	.021	15	.054	25	.066
6	.000	16	.049	26	.141
7	-.021	17	.030	27	.213
8	-.038	18	.000	28	.272
9	-.044	19	-.034	29	.308
10	-.040	20	-.063	30	.318

Computation of Fourier Coefficients, Sheet 1

Example 1 $\omega_o = 3.6$

$(2n-1)\omega_o/36$	$-I(\omega)\times 1000$				
n=1 .1	60	1+18 70	.087	6	
2 .3	220	2+17 250	.259	65	
3 .5	410	3+16 455	.422	192	
4 .7	800	4+15 865	.574	495	
5 .9	1125	5+14 1205	.707	852	
6 1.1	1180	6+13 1280	.820	1049	
7 1.3	1000	7+12 1140	.906	1029	
8 1.5	640	8+11 840	.964	810	
9 1.7	430	9+10 720	.996	718	
10 1.9	290		9	5216	
11 2.1	200		$a_1 = -.577$		
12 2.3	140	1+9 490	10+18 300	190	.174 33
13 2.5	100	2+8 860	11+17 230	630	.500 315
14 2.7	80	3+7 1410	12+16 185	1225	.766 940
15 2.9	65	4+6 1980	13+15 165	1815	.939 1701
16 3.1	45	5 1125	14 80	1045	1.000 1045
17 3.3	30			9	4034
18 3.5	10			$a_2 =$	$-.448$

Computation of Fourier Coefficients, Sheet 2

Example 1 $\omega_0 = 3.6$

1 60	2 220	3 410	
6 1180	5 1125	4 800	
13 100	14 80	15 65	
18 10	17 30	16 45	
1350	1455	1320	Add
7 1000	8 640	9 430	
350	815	890	Subtract
12 140	11 200	10 290	
210	615	600	Subtract
.259	.707	.964	
54	435	578	1067 - 9 = -.119

1 60	2 220	3 410	4 800	
10 290	11 200	12 140	13 100	
350	420	550	900	Add
9 430	8 640	7 1000	6 1180	
-80	-220	-450	-280	Subtract
18 10	17 30	16 45	15 65	
-90	-250	-495	-345	Subtract
.342	.866	.984	.642	
-31	-216	-486	-222	-955 - 9 = +.106

Computation of h(t), Sheet 1

Example 1 $\omega_o = 3.6$ $a_1 = -.577$ $a_2 = -.448$ $a_3 = -.119$ $a_4 = +.106$

$t = \frac{n\pi}{6\omega_o} = .145n$	Multiply by $-\omega_o a_1$ $+2.078$	$\omega_o a_2$ -1.611	$-\omega_o a_3$ $+.428$	$\omega_o a_4$ $+.3815$	Partial sums +	Partial sums -	h(t)
0 .00	———	———	———	———	———	———	.000
1 .15	.104 .216	.051 -.082	.054 .015	.025 .010	.241	.082	.159
2 .29	.197 .410	.090 -.145	.059 .025	.044 .017	.452	.145	.307
3 .44	.269 .559	.108 -.174	.069 .030	.051 .019	.608	.174	.434
4 .58	.314 .652	.099 -.159	.062 .027	.045 .017	.696	.159	.537
5 .73	.330 .685	.065 -.105	.057 .016	.026 .010	.711	.105	.606
6 .87	.318 .660	———	———	———	———	———	.660
7 1.02	.279 .580	-.077 .124	-.040 -.017	-.028 -.011	.704	.028	.676
8 1.16	.225 .467	-.158 .254	-.073 -.032	-.050 -.019	.721	.051	.670
9 1.31	.161 .334	-.237 .382	-.090 -.039	-.059 -.023	.716	.062	.654
10 1.45	.098 .204	-.288 .465	-.085 -.036	-.053 -.020	.669	.056	.613
11 1.60	.043 .088	-.316 .509	-.054 -.023	-.032 -.012	.597	.035	.562
12 1.75	———	-.318 .512	———	———	———	———	.512
13 1.89	-.027 -.056	-.292 .470	.071 .030	.036 .014	.514	.056	.458
14 2.04	-.040 -.083	-.244 .393	.149 .064	.067 .026	.483	.083	.400
15 2.18	-.039 -.081	-.180 .290	.221 .095	.083 .032	.417	.081	.336
16 2.33	-.029 -.060	-.113 .182	.279 .119	.079 .030	.331	.060	.271
17 2.48	-.014 -.029	-.050 .081	.312 .134	.051 .019	.234	.029	.205
18 2.62	———	———	.318 .136	———	———	———	.136

Computation of h(t), Sheet 2

Example 1 ω_o = 3.6 a_1 = -.577 a_2 = -.448 a_3 = -.119 a_4 = +.106

$t=\frac{n\pi}{6\omega_o}$ = .145 n	Multiply by $-\omega_o a_1$ +.2078	$\omega_o a_2$ -1.611	$-\omega_o a_3$ +.428	$\omega_o a_4$ +.3815	Partial sums +	Partial sums -	h(t)
19 2.77	.011 .023	.034 -.055	.296 .127	-.068 -.026	.150	.081	.069
20 2.91	.017 .035	.049 -.079	.250 .107	-.144 -.055	.142	.134	.008
21 3.06	.018 .037	.049 -.079	.185 .079	-.216 -.082	.116	.161	-.045
22 3.20	.014 .029	.037 -.060	.119 .051	-.275 -.105	.080	.165	-.085
23 3.35	.007 .015	.019 -.031	.053 .023	-.510 -.118	.038	.149	-.111
24 3.50	———	———	———	-.518 -.121	———	———	-.121
25 3.64	-.006 -.012	-.015 .024	-.036 -.015	-.298 -.117	.024	.144	-.120
26 3.79	-.010 -.021	-.024 .039	-.054 -.023	-.255 -.099	.039	.143	-.104
27 3.94	-.011 -.023	-.025 .040	-.053 -.023	-.191 -.075	.040	.121	-.081
28 4.08	-.008 -.017	-.020 .032	-.041 -.018	-.122 -.048	.032	.083	-.051
29 4.23	-.005 -.010	-.010 .016	-.031 -.013	-.055 -.022	.016	.045	-.029
30 4.37	———	———	———	———	———	———	.000

APPENDIX III

In order to approximate the convolution integral

$$\theta_o(t) = \int_o^t h(t-x)\, \theta_i(x)\, dx \qquad (12)$$

Tustin[11] suggests the following procedure. Break up $\theta_i(t)$ into impulses occurring at equally spaced times. In Figure 14(a), the impulse b_2 has an average height of (.25 + .50)/2 = .375 units and a base of .50 - .25 = .25 seconds; it is replaced by an impulse of magnitude .375 x .25 = .094 occurring at (.25 + .50)/2 = .375 seconds. Similarly b_4 is replaced by an impulse of magnitude .219 occurring at .875 seconds.

Write h(t) as a time series the terms of which are its values at .25 second intervals starting with t = 0; this is the top line of Table 1. Multiply each term of this series by the magnitude of an impulse and translate the result to the right so that the first term lies under the time the impulse was considered to have occurred. Impulse b_2 corresponding to n = 2 has as its first non-zero term .094 x .300 = .028 (= 28 in the table since all values are multiplied by 1000 as a matter of convenience) and its first (zero) term is entered under t = .375 and opposite n = 2 in the table. Similarly the first non-zero term of b_4 equals .219 x .300 = .066 and its first (zero) term is entered under t = .875 and opposite n = 4.

The terms of the resulting $b_n x h(t)$ series are then added vertically to give the totals at the bottom of Table 1. These totals represent $\theta_o(t)$ for the values of t under which they lie. The result of this computation is plotted as Figure 14(b).

The time interval between terms of the h(t) series can be as large as will give an adequate representation but should be equal to or an integral submultiple of the time intervals between impulses. These latter intervals can be chosen quite large since the form of an impulse is immaterial if it has been completed before the system has responded appreciably.

Table 2

Approximating the Convolution Integral

(All tabular values except t and b_n are x 1000)

h(t) = 0	300	501	620	677	670	610	520	410	290	184	90	0	-70	-112
t =	.125	.375	.625	.875	1.125	1.375	1.625	1.875	2.125	2.375	2.625	2.875	3.125	3.375
n b_n														
1 .031	0	9	16	19	21	21	19	16	13	9	6	3	0	-2
2 .094		0	28	47	58	64	63	57	49	38	27	17	8	0
3 .156			0	47	78	97	106	105	95	81	64	45	29	14
4 .219				0	66	110	136	148	147	133	114	90	63	40
5 .282					0	84	141	174	190	188	171	146	115	82
6 .344						0	105	172	213	232	230	210	179	141
7 .406							0	122	204	252	275	272	248	211
8 .468								0	141	235	290	318	314	286
9 .530									0	159	266	329	360	356
10 .594										0	178	298	368	402
11 .655											0	197	329	407
12 .719												0	216	360
13 .780													0	234
14 .844														0
$\theta_o(t)$	0	9	44	113	223	376	568	794	1042	1327	1621	1925	2229	2531